Biogeosciences Discuss., doi:10.5194/bg-2016-548, 2017
Manuscript under review for journal Biogeosciences
Published: 11 January 2017

Biogeosciences Discussions
Open Access
EGU

On the long-range offshore transport of organic carbon from the Canary Upwelling System to the open North Atlantic

Elisa Lovecchio[1], Nicolas Gruber[1], Matthias Münnich[1], and Zouhair Lachkar[2]

[1]ETH-Zürich, Universitätstrasse 16, 8092 Zürich, Switzerland
[2]Center for Prototype Climate Modeling, New York University Abu Dhabi, Abu Dhabi, UAE

Correspondence to: Elisa Lovecchio (elisa.lovecchio@usys.ethz.ch)

Abstract. A compilation of measurements of Net Community Production (NCP) in the upper waters of the eastern subtropical North Atlantic had suggested net heterotrophic conditions, purportedly supported by the lateral export of organic carbon from the adjacent highly productive Canary Upwelling System (CanUS). Here, we quantify and assess this lateral export using the Regional Ocean Modeling System (ROMS) coupled to a Nutrient, Phytoplankton, Zooplankton, and Detritus (NPZD) ecosystem model. We employ a new Atlantic telescopic grid with a strong refinement towards the north-western African shelf to combine an eddy-resolving resolution in the CanUS with a full Atlantic basin perspective. Our climatologically forced simulation reveals an intense offshore flux of organic carbon that transports over the whole CanUS about 19 Tg C yr^{-1} away from the nearshore 100 km, amounting to more than a third of the NCP in this region. The offshore transport extends beyond 1500 km into the subtropical North Atlantic, along the way adding organic carbon to the upper 100 m at rates of between 8 % and 34 % of the alongshore average NCP as a function of offshore distance. Although the divergence of this lateral export of organic carbon enhances local respiration, the upper 100 m layer in our model remains net autotrophic in the entire eastern subtropical North Atlantic. However, the vertical export of this organic carbon and its subsequent remineralization at depth makes the vertically-integrated NCP strongly negative throughout this region, with the exception of a narrow band on the north-western African shelf. The magnitude and efficiency of the lateral export varies substantially between the different subregions. In particular, the central coast near Cape Blanc is particularly efficient in collecting organic carbon on the shelf and subsequently transporting it offshore. In this central subregion, the offshore transport adds to the upper 100m as much organic carbon as nearly 60 % of the local NCP, giving rise to a sharp peak of offshore respiration that extends to the middle of the gyre. Our results emphasize the fundamental role of the lateral redistribution of the organic carbon for the maintenance of the heterotrophic activity in the open sea.

Biogeosciences Discuss., doi:10.5194/bg-2016-548, 2017
Manuscript under review for journal Biogeosciences
Published: 11 January 2017

1 Introduction

Owing to the dominance of the sinking flux of particulate organic carbon (POC), the ocean's biological pump is often simplified to a one-dimensional vertical process, consisting of the production of POC in the euphotic zone, its vertical export by gravitational sinking, and the remineralization of this organic carbon in the aphotic zone (e.g., Sarmiento and Gruber, 2006). Reflecting this simplified view, most biogeochemical models currently used in the context of global climate models consider only the vertical export pathway for POC, thus neglecting its potential lateral transport by horizontal advection and diffusion (e.g., Aumont et al., 2003; Moore et al., 2004; Galbraith et al., 2010; Shigemitsu et al., 2012).

Nevertheless, the horizontal transport of POC can be substantial, even in the presence of vertical sinking speeds of POC of 10 m day^{-1} or more. This is especially the case in places characterized by high lateral advective velocities (Helmke et al., 2005) and the presence of upward vertical transports that can help to maintain high organic matter concentrations in the upper ocean against its gravitational sinking (Plattner et al., 2005). In addition, resuspension of bottom sediments and can create nepheloid layers that can transport POC over hundreds of kilometers (Ohde et al., 2015; Inthorn et al., 2006a; Falkowski et al., 1994). A further important contribution to the lateral transport of organic carbon is that of dissolved organic carbon (DOC), estimated to account for 20 % of the export to depth and for about 10 % of the respiration rates in the deep ocean (Hansell, 2002; Arítegui et al., 2002; Ducklow et al., 2001). As a consequence of these transport processes, the different organic carbon pools get redistributed laterally from regions of excess production to regions of intense remineralization and burial (Inthorn et al., 2006b; Hwang et al., 2008), giving rise to a complex pattern of organic carbon cycling.

Such a lateral connection between organic carbon sources and sinks in the marine environment is at the heart of a long-standing controversy regarding the net metabolic state of the upper ocean in the oligotrophic subtropical gyres (Williams et al., 2013; Duarte et al., 2013; Ducklow and Doney, 2013). Based on a compilation of bottle-incubations that measure the net changes of oxygen over time, Duarte and Agustí (1998) and Del Giorgio and Duarte (2002) had suggested that oligotrophic systems, and particularly the near-surface layer in the center of the subtropical gyres tend to be heterotrophic. They suggested, although without any quantification, that this net heterotrophy is sustained by organic carbon that is supplied laterally to the center of the gyres from the adjacent more productive regions. This claim has fueled an intense debate, ranging from a discussion of the suitability of oxygen incubation experiments to assess the metabolic state of the ocean, to the question of whether it is actually possible to supply such a large amount of organic carbon through lateral processes (Williams et al., 2013; Duarte et al., 2013; Ducklow and Doney, 2013).

A key role in this debate is played by the Eastern Boundary Upwelling Systems (EBUS), as these very productive continental margins (Chavez and Messié, 2009; Carr, 2002) are straddling the oligotrophic subtropical gyres. They thus may provide the source of the organic carbon that fuels the purportedly heterotrophic conditions in the latter regions (Liu et al., 2010; Walsh, 1991). In fact, with most of the NCP measurements indicating net heterotrophic stemming from the eastern subtropical North Atlantic (Duarte et al., 2013), the Canary Upwelling System (CanUS) has been at the center of studies addressing the offshore transport of organic carbon (e.g. Pelegrí et al., 2005).

Biogeosciences Discuss., doi:10.5194/bg-2016-548, 2017
Manuscript under review for journal Biogeosciences
Published: 11 January 2017

Located on the eastern side of the North Atlantic Ocean, the CanUS spans the region between the North African Coast between 9°N and 33°N and the adjacent portion of the North Atlantic Gyre (Váldes and Déniz-González, 2015). A complex circulation pattern determines strong subregional differences in the CanUS in terms of circulation, mesoscale activity, seasonality of upwelling and biology (Arístegui et al., 2009). The high productivity in the CanUS is sustained both by local coastal upwelling and by meridional alongshore advection of nutrients (Carr and Kearns, 2003; Auger et al., 2016). Sufficiently long water residence times in the nearshore region, favorable light and temperature conditions also contribute to sustain high levels of production (Lachkar and Gruber, 2011). Dedicated local surveys have demonstrated that the export of coastally produced organic carbon from the CanUS shelf to the open sea can be intense (Pelegrí et al., 2005; Arístegui et al., 2003) and include living organisms (Brochier et al., 2014). On top of the mean Ekman transport, persistent filaments originating on the CanUS shelf have been reported to be able to export up to 50 % of the coastally produced organic matter as far as several hundreds of km offshore (Gabric et al., 1993; Ohde et al., 2015). Due to these fluxes, a substantial amount of coastally produced organic carbon in the CanUS escapes remineralization in the nearshore region and is advected offshore towards the center of the North Atlantic Gyre (Fischer et al., 2009; García-Muñoz et al., 2005). Estimates from multiple local surveys indicate that on average about 16 % of the coastal production by phytoplankton is laterally exported to the open sea (Duarte and Cebrián, 1996). The CanUS constitutes therefore a good potential candidate source region for the organic carbon required to fuel the purportedly heterotrophic conditions in the subtropical North Atlantic. However, despite its potential impact on the offshore biological activity (Alonso-González et al., 2009; Álvarez Salgado et al., 2007), the magnitude and range of the total long-range offshore transport of organic carbon in the CanUS is still poorly quantified.

The quantification of this export is notoriously difficult to achieve through in-situ studies owing to the intermittency of the transport and the importance of eddies, filaments and other turbulent structures (e.g., Peliz et al., 2004; Nagai et al., 2015), providing models an opportunity to fill the gap. These models need to have relatively high resolution, in order to resolve this mesoscale dynamics, forcing most studies to employ regional models instead of global ones. But so far, relatively few high resolution modeling studies have focused on the CanUS compared to other upwelling regions and even fewer have employed a fully coupled biogeochemical model (Auger et al., 2016; Fischer and Karakaş, 2009; Lachkar and Gruber, 2011).

Most of the conducted work regarding the lateral redistribution of organic carbon relied on regional configurations of the Regional Ocean Modeling System (ROMS) and tended to focus on sub-aspects of the offshore transport of organic matter, either by focusing on sub-regions, or by focusing on the offshore transport of a subset of constituents. In the most recent study, Auger et al. (2016) used a regional ROMS configuration coupled to the biogeochemical/ecological module PISCES (Pelagic Interactions Scheme for Carbon and Ecosystem Studies) to highlight the important role of the lateral redistribution of nutrients and phytoplankton on the CanUS shelf for determining the complex seasonal pattern of chlorophyll and for the fueling of the persistent Cape Blanc offshore bloom. Despite the specific focus on phytoplankton, their analysis extended the work of previous studies which concentrated on the lateral transport of organic carbon in limited portions of the CanUS. Among these studies, Sangrà et al. (2009) estimated the integrated lateral export and production of organic carbon in the eddy corridor shed by the Canary Archipelago and its potentially big impact on the region combining a physical ROMS simulation with estimates of carbon concentration in the eddies based on a few eddy surveys. With a ROMS-driven Lagrangian experiment,

Biogeosciences Discuss., doi:10.5194/bg-2016-548, 2017
Manuscript under review for journal Biogeosciences
Published: 11 January 2017

Brochier et al. (2014) studied the observed biological coupling between the African coast and the Canary Islands in terms of the offshore transport of ichtyoplankton (eggs and larvae of fish) by filaments. With a wider focus area, Fischer and Karakaş (2009) employed a relatively simple Nutrient Phytoplankton Zooplankton and Detritus (NPZD) model coupled to their regional configuration of ROMS to study the role of sinking speeds in the vertical export of organic carbon to the deep ocean in the CanUS. While these studies demonstrated clearly the importance of offshore fluxes in the CanUS, they failed to address the total long-range transport of organic carbon from the CanUS into the oligotrophic subtropical North Atlantic. This is largely due to the limited offshore dimension of the regional ROMS configurations, with typical offshore extents of a few hundred kilometers only.

Here we overcome this limitation and provide a first comprehensive quantification of the long-range lateral fluxes of organic carbon from the CanUS shelf to the open North Atlantic using a new regional configuration of ROMS. This configuration employs a basin-scale telescopic grid that allows us to model the whole Atlantic basin in a continuous manner, while maintaining a full eddy resolving resolution in the region of study. Thus, this configuration is ideally suited to assess the long-range transport owing to its fully resolving all scales. Furthermore, this permits us to push the lateral boundaries far away from the region of interest, thus avoiding the many challenges and distortions associated with the lateral boundary conditions in regional studies. We couple this physical setup with a NPZD-type ecosystem model that fully resolves the three-dimensional dynamics of the organic carbon redistribution. In particular, the vertical sinking of the different pools of organic matter is explicitly solved for, permitting us to advect and diffuse POC in the vertical and horizontal directions. Our results show that the organic carbon offshore flux in the CanUS significantly enhances the carbon availability of the open waters. Substantial subregional differences in the pattern of lateral and vertical fluxes and key pathways for the carbon lateral redistribution are highlighted and discussed in the context of the previous research.

2 Methods

2.1 Model configuration

We employ the UCLA-ETH version of the Regional Ocean Modeling System (ROMS) (Shchepetkin and McWilliams, 2005), coupled with the Nutrient, Phytoplankton, Zooplankton and Detritus (NPZD) biogeochemical ecosystem module of Gruber et al. (2006). ROMS solves the 3D hydrostatic primitive equations of flow on a discretized curvilinear grid, using terrain following vertical coordinates (sigma levels). Surface elevation, barotropic and baroclinic horizontal velocity components, potential temperature and salinity are its prognostic variables. Vertical mixing is parameterized by the K profile parameterization (KPP) scheme (Large et al., 1994).

The NPZD ecosystem module is a nitrogen-based model with two limiting nutrients, i.e., nitrate and ammonium, one class of phytoplankton, one class of zooplankton and two detritus pools, i.e., a small one that sinks very slowly, and a large one that is subject to more rapid sinking (Gruber et al., 2006). These components plus a dynamic chlorophyll-to-carbon ratio form the seven prognostic variables of the nitrogen component of the model. An additional four state variables have been added to reflect the cycling of carbon and oxygen, namely dissolved inorganic carbon (DIC), alkalinity, and mineral $CaCO_3$ (Hauri

Biogeosciences Discuss., doi:10.5194/bg-2016-548, 2017
Manuscript under review for journal Biogeosciences
Published: 11 January 2017

et al., 2013; Turi et al., 2014; Lachkar and Gruber, 2013). The carbon and oxygen cycles are linked to the nitrogen cycle by fixed stochiometric ratios. Thus, the fluxes of organic carbon diagnosed in our model are actually the fluxes of organic nitrogen multiplied by the C:N ratio assumed in the model, i.e., 117:16.

Particulate organic carbon in the model, i.e., the sum of phytoplankton, zooplankton, and the two detritus pools, is subject to advection and diffusion in vertical and horizontal directions, as well as explicit vertical sinking (the latter does not apply to zooplankton, however). Sinking velocities for phytoplankton, small detritus and large detritus are 0.5 m day^{-1}, 1 m day^{-1}, 10 m day^{-1}, respectively (see Gruber et al. (2011) for a complete set of parameters). Particulate organic carbon is formed through phytoplankton growth and is lost through zooplankton respiration and the remineralization of the two detrital pools. Within the organic carbon pool, phytoplankton mortality feeds into the small detritus pool, while zooplankton mortality and phytoplankton excretion is routed to both the small and large detritus pools with constant proportions. Coagulation of phytoplankton with small detritus also forms large detritus, while no disaggregation is considered in our NPZD model, i.e., large detritus cannot disaggregate back into small detritus. Bacterial remineralization of organic matter is modeled as an implicit process through the definition of constant remineralization rates and takes place both in the water column and in the sediments. The sediments act as a temporal buffer in our model, receiving the organic matter from the water column, and then slowly remineralizing it back to its inorganic constituents, which are released back immediately to the overlying water column. Neither burial nor sediment resuspension is considered.

In order to optimally model the long-range transport of organic matter from the CanUS to the open North Atlantic, we employ a newly developed Atlantic telescopic grid (Figure 1) that covers the full Atlantic basin (-60°N to 70°N) while having a strong focus in resolution toward the north-western African coast. This was achieved using a conformal mapping that moves one pole of the ROMS grid over Northwest Africa (4°W, 20°N) and the other over Central Asia (75°E, 37°N). The grid has a dimension of 813 x 397 with a resolution that goes from a full eddy resolving 4.7 km near the African coast to a relatively coarse 50 km in the western South Atlantic and in the Caribbean (Figure 1). Within the CanUS region as defined in our analysis, the resolution ranges between 4.7 km at the coast and 19.5 km. In the vertical, we are considering 42 terrain following (sigma) levels with a surface refinement that allows to have a better vertical resolution in the euphotic layer. We use a new vertically stretched grid that transitions more rapidly from a pure terrain following orientation to a more horizontal orientation in order to reduce spurious mixing in the stratified open ocean.

2.2 Boundary Conditions

The coupled ROMS+NPZD model was run with monthly mean climatological forcing at the surface including the fluxes of heat and freshwater, solar shortwave radiation, wind stress and atmospheric pCO_2. All forcings were derived from ERA-Interim reanalysis (Dee et al., 2011), with the exception of atmospheric pCO_2, which was computed from the GLOBALVIEW marine boundary layer product (GLOBALVIEW-CO_2 (2011), see Landschützer et al. (2014) for details). A detailed description of the data sources used for the forcing is provided in Appendix A: Datasets, Table A1a and Table A1b. We next describe some corrections we had to apply to the forcing.

Biogeosciences Discuss., doi:10.5194/bg-2016-548, 2017
Manuscript under review for journal Biogeosciences
Published: 11 January 2017

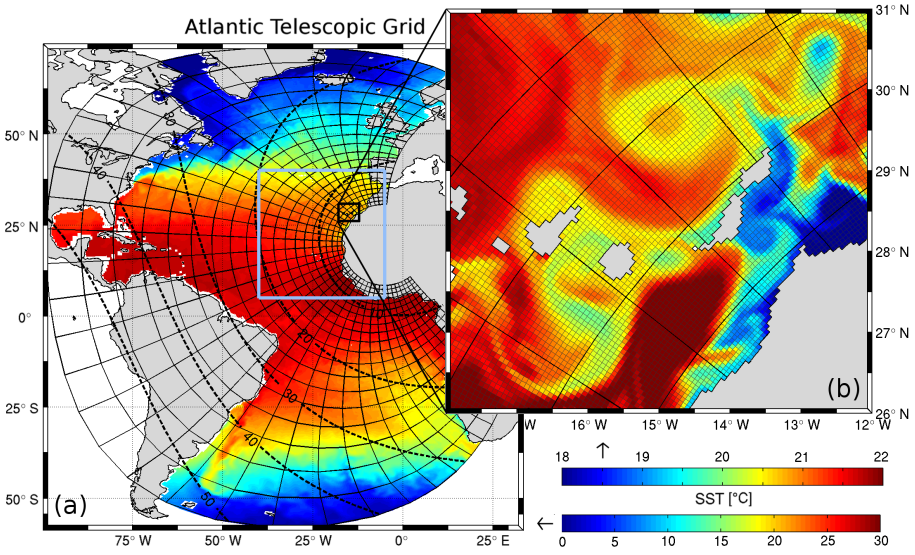

Figure 1. Map of the domain of the Atlantic telescopic grid together with a snapshot of the modeled sea-surface temperature. (a) Map of the full domain. Shown are every 20th grid line. Dashed isolines indicate the resolution of the grid in km. The light blue square highlights the region of interest used for the CanUS plots throughout the whole paper [5°N to 40°N, and -40°E to -5°E]; the black square indicates the region used for the zoomed-in subplot (b) Zoom on the Canary Islands region with actual grid resolution. Every 20th line is plotted thicker, corresponding to the grid lines shown in (a). As a point of reference, the island of Gran Canaria has a diameter of about 45 km.

The ERA-Interim-based shortwave radiation and total heat flux fields have been shown to be biased high in regions of persistent cover with stratocumulus clouds (Brodeau et al., 2010). This is particularly relevant in the southern subregion of the CanUS, where stratocumulus are very pervasive and not well represented in the ERA-Interim reanalyses. We thus apply corrections to the original ERA-Interim reanalysis fields, taking advantage of the work by the Drakkar community (Dussin et al., 2016). They have already developed corrected forcing fields, i.e., the Drakkar Forcing Sets (DFS) (Dussin et al., 2016) on the basis of the ERA-Interim reanalysis (Brodeau et al., 2010), providing the corrected fields for the downwelling surface shortwave radiation (DSWR) and downwelling surface longwave radiation (DLWR). We thus compute correction masks ourselves, using the difference between the DFS and the uncorrected ERA-Interim data sets as the basis. Concretely, we first computed monthly means of the DFS daily climatology DSWR and DLWR. The monthly climatological means of the same two variables from ERA-Interim for the period were then used as a reference to calculate correction masks (C) for each month by simply differencing, i.e., $C_{dswr} = ERA_{dswr} - DFS_{dswr}$ and $C_{dlwr} = ERA_{dlwr} - DFS_{dlwr}$. These correction masks were then regridded to our grid and applied to our ERA-Interim-derived monthly climatological mean forcing solar radiation (S) and total heat flux (TH) so that $S' = S - C_{dswr}$ and $TH' = TH - (C_{dlwr} + C_{dswr})$.

Another correction to the forcing regards the regions with sea ice cover at the northern boundary of the domain. Here we account for freshwater and latent heat fluxes associated with sea ice formation and melting by correcting the surface fluxes of the model forcing. An offline correction for the forcing was calculated from the ERA-interim sea ice fraction (c) and NSIDC

Biogeosciences Discuss., doi:10.5194/bg-2016-548, 2017
Manuscript under review for journal Biogeosciences
Published: 11 January 2017

sea ice drift ($\boldsymbol{u}$) monthly climatologies. Using these two datasets, the corrections to the freshwater flux (F_{fw}) were calculated according to Haumann et al. (2016), but simplified by using monthly mean climatologies, a constant sea ice thickness h_0 = 1.5 m and a sea ice density ρ_{ice}= 910 kg m^{-3}. An analogous equation was used to calculate the correction to the heat flux (F_h), so that: $F_h = \rho_{ice} L \cdot h_0(\partial(Ac)/\partial t + \boldsymbol{\nabla}(Ac\boldsymbol{u}))$ where A is the grid box area, and L the latent heat of fusion of water. The heat flux is constrained throughout the model simulation, so that the surface temperature cannot drop below the freezing temperature (Steele et al., 1989), which prevents strong heat loss in sea ice covered areas.

River runoff in the form of monthly climatological data (Dai et al., 2009) was also added to the freshwater fluxes. River sources were regridded to the closest ocean grid point and spread to a number of adjacent ocean grid points that depends the order of magnitude of the incoming flux to avoid numerical problems.

The model was run with open lateral boundaries at all grid boundaries confined by water, including at the Strait of Gibraltar. These climatological monthly lateral boundary conditions were prepared the same way as in previous studies (Lachkar and Gruber, 2013). A detailed description of the datasets used for the boundary conditions can be found in Appendix A: Datasets, Table A2.

2.3 Simulation and Analysis

The model was initialized to be at rest with temperature, salinity, nitrate, and the inorganic carbon parameters corresponding to the mean climatological value of December and January. The remaining biogeochemical variables were initialized to small non-zero values. The model was then run forward in time for a total of 35 years, using the monthly climatological forcing described above. We use the first 30 years as spin-up, and undertake our analyses using the last 6 years (years 30 to 35) of the simulation. This permits us to obtain a good representation of the climatological mean state of the CanUS, i.e., to average out the substantial intrinsic variability present in the setup.

To quantify the offshore transport of organic carbon including all its biogeochemical transformations, we undertake a full budget analysis, calculating all fluxes of organic carbon within each grid box and between all adjacent boxes. Physical fluxes through the boundaries of the boxes include advective fluxes in the three directions, vertical mixing (eddy-diffusive) fluxes and the vertical sinking flux. Convective mixing was disregarded as it is small. The net biological flux of organic carbon within each box is equivalent to the net community production (NCP), i.e., the net amount of carbon added or removed by biological activity, computed by summing all organic carbon production processes (phytoplankton growth) minus the sum of all processes that convert organic carbon back to inorganic forms (respiration and remineralization).

For the whole CanUS, defined as the region between 9.5°N and 32°N, we have defined two layers of 3-dimensional boxes. Each depth layer has a constant thickness of 100 m, very close to the mean depth of the euphotic layer in the CanUS region (98.7 m), so that our analysis spans in total the first 200 m of depth. Each depth layer is subdivided into the same five offshore boxes up to 2000 km distance from the north-west African coast according to the following ranges of distances: (1) 0 to 100 km from the coast, narrow “coastal box” directly influenced by the coastal upwelling; (2) from 100 km to 500 km offshore; (3) from 500 km to 1000 km offshore; (4) from 1000 km to 1500 km offshore; (5) from 1500 km to 2000 km offshore.

Biogeosciences Discuss., doi:10.5194/bg-2016-548, 2017
Manuscript under review for journal Biogeosciences
Published: 11 January 2017

To highlight the different roles of three fundamental zonal bands in the CanUS, we have divided the EBUS into three subregions (Southern, Central, Northern), maintaining for each subregion the same five offshore domains as for the previous analysis. Subregional boundaries were placed at 17°N and 24.5°N. The subregional box analysis was done for the euphotic layer only (0 m -100 m).

3 Evaluation

The model represents well the general circulation of the whole Atlantic Basin with a particularly good agreement of the modeled Sea Surface Height (SSH) with the observed one (Appendix B: Supplementary figures, Figure B1). This is remarkable given the lateral extension and the stretching of the grid on which ROMS was run. Less well modeled is the SSH in the eastern side of the North Atlantic Gyre and in particular in the Gulf Stream region. Especially problematic is the too late separation of the Gulf Stream from the North American coast, a problem shared with many ocean general circulation models. These deviations are likely connected to our relatively coarse resolution in that part of the domain (Figure 1). But they occur far away from the region of interest, and are thus considered tolerable for the purpose of this study. The SST pattern is also well represented; differences are concentrated in the near equatorial region and are probably connected to a weaker equatorial circulation and a possible residual overestimation of the net heat flux in this region despite the correction we applied to the original forcing.

A zoom on the North-East Atlantic region allows us to evaluate the representation of the variables in our region of study, i.e., the CanUS. Here, modeled annual mean SST (Figure 2a) and SSH (Figure 2b) are well reproduced with a clearly visible signature of low SSH and cold water along the African coast as a result of the Ekman upwelling. Some differences in SSH are discernible at the northern boundary owing to the eastward flowing Azores Current being located slightly more south than observed. A slight shift south is also visible at the southern boundary. Despite the stratus cloud correction, the modeled SSTs are still a bit too warm in the southern sector of the CanUS, but differences between model and observations rarely exceed 1°C and the latter are very confined to the nearshore. Modeled Sea Surface Salinity (SSS, Figure 2c) well reproduces the observed fields; relevant negative differences are only observed in the southern CanUS, in correspondence to the warm SST bias, with a consequent compensation of the density.

The modeled annual mean Mixed Layer Depth (MLD, Figure 2d) shows sharper gradients than the observed Argo-based MLD product, even tough the general pattern is consistent with the observations. Deeper than observed values of the MLD are visible in the northern sector of the CanUS and in the nearshore waters of the southern sector of the CanUS. It is also worth noting that the Argo dataset is provided on a relatively low resolution grid, i.e., 2°x 2°, and thus is likely underestimating gradients. In addition, the float coverage in Eastern Boundary Current system is relatively low, owing to the strong currents and the offshore transport, making the Argo-based MLD product vulnerable for biases in these regions. Nevertheless, some of the differences are likely real, as they appear also in other products. This is particularly the case in the nearshore region of the southern CanUS. Also the general overestimation of MLD by the model along a long strip extending southwestward from

Biogeosciences Discuss., doi:10.5194/bg-2016-548, 2017
Manuscript under review for journal Biogeosciences
Published: 11 January 2017

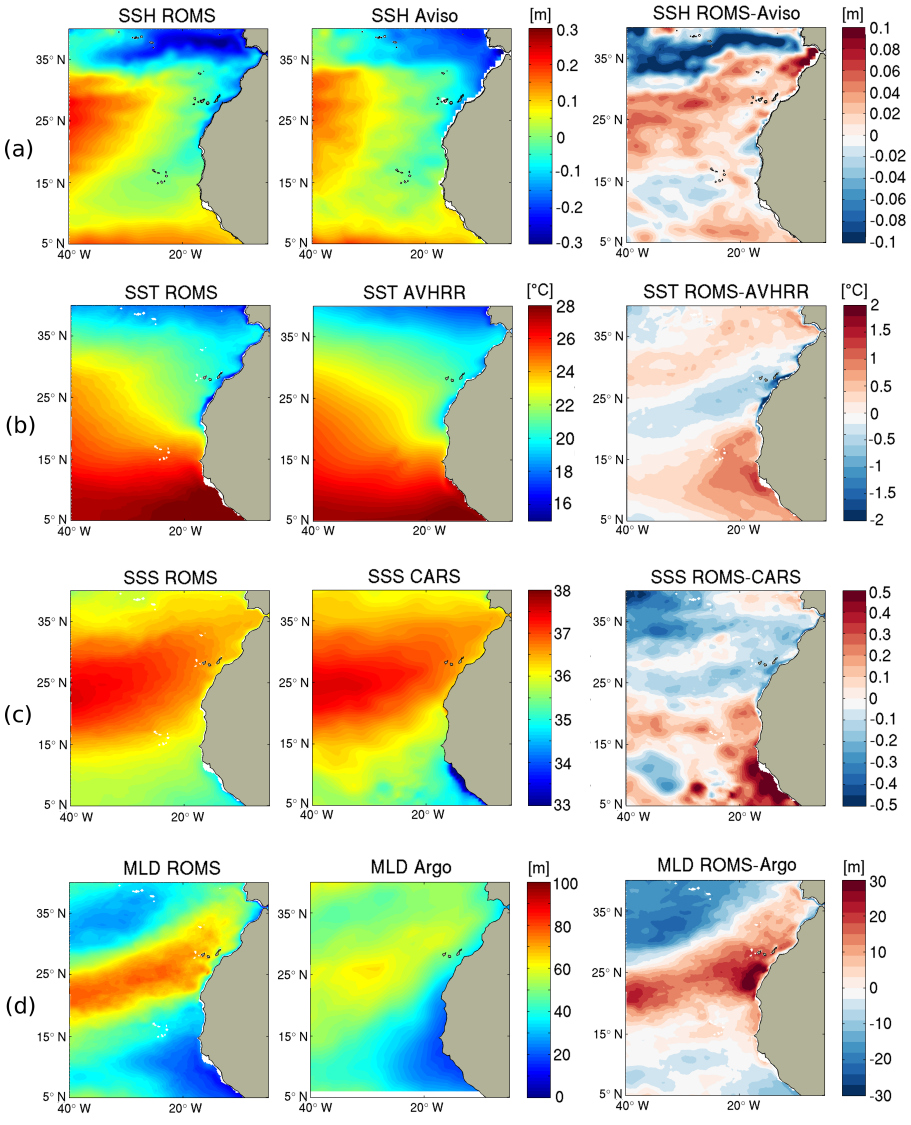

Figure 2. Evaluation of the model simulated annual mean fields in the CanUS region. (a) Sea Surface Height (SSH); (b) Sea Surface Temperature (SST); (c) Sea surface Salinity (SSS); (d) and Mixed Layer Depth (MLD). Left column: ROMS output; Middle column: observations; Left column: difference between model and data. A detailed description of the data used for the evaluation is provided in Appendix A: Datasets, Table A3.

the Canary Island is likely real, possibly connected to the biases in the position of the large-scale currents as evidenced by the biases in SSH (Figure 2a).

The modeled annual mean circulation averaged over the first 100 m of depth corresponds well to the system of currents described schematically in Mackas et al. (2006) and Arístegui et al. (2009) (Figure 3). The Canary Current System is delimited

Biogeosciences Discuss., doi:10.5194/bg-2016-548, 2017
Manuscript under review for journal Biogeosciences
Published: 11 January 2017

on the northern edge by the eastward flowing Azores Current and on the southern edge by the eastward flowing North Equatorial Counter Current. Within these boundaries two currents flow in opposite directions along the African coast: the Canary Current flows southward between Cape Beddouza (33°N) and Cape Blanc (21°N), while the weaker and seasonal Mauritanian current flows northward between 10°N and Cape Blanc (21°N). Next to Cape Blanc, both the Canary Current and the Mauritanian Current detach from the coast and flow offshore forming the Cape Verde frontal zone, a natural boundary for the flow of water masses and tracers in the region. This front divides the region into a northern so-called Moroccan subregion and a southern Mauritanian-Senegalese subregion that differ in both physical circulation and biological activity.

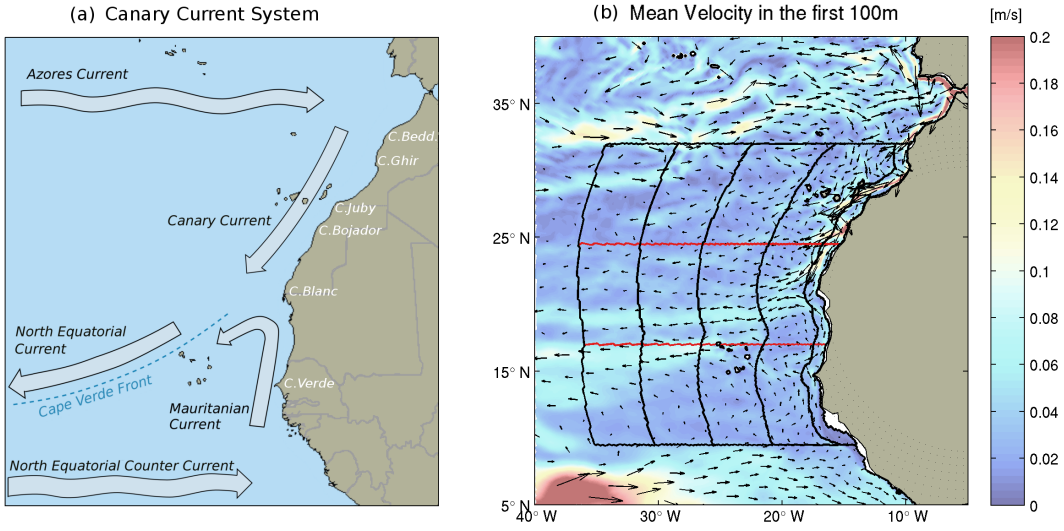

Figure 3. Maps of the circulation of the Canary Current System. (a) Schematic depiction with major currents adapted from Arístegui et al. (2009); (b) Modeled system of currents based on the vertically averaged flow in the first 100 m depth. Black lines represent the boundaries of the budget analysis regions for the Full CanUS analysis, while the red lines indicate the 2 extra boundaries for the subregional budget analysis. The Full CanUS covers the region between 32°N and 9.5°N. Subregional boundaries are at 17°N and 24.5°N. From East (African coast) to West boxes span the following ranges of offshore distances: 0 km-100 km, 100 km-500 km, 500 km-1000 km, 1000 km-1500 km, 1500 km-2000 km.

The overall gradients in annual mean sea surface chlorophyll (CHL) are well captured by the model (Figure 4a). This is especially the case in the northern CanUS where the absolute values are captured well, even though the model is slightly biased low. Less well captured is the surface CHL in the productive southern sector of the CanUS, where the model underestimates the observed surface CHL substantially. This is also the region in which the model is biased too warm and salty, suggesting that this low surface CHL bias is real and not simply a result of uncertainties in the satellite retrievals in this region, owing to frequent cloud cover and difficult optical conditions in the water column.

Our analysis of the vertical CHL distribution reveals that in the southern CanUS the modeled CHL has a deep maximum located between 20 m and 50 m depth, while little of the CHL is found in the surface layer (see Appendix B: Supplementary

Biogeosciences Discuss., doi:10.5194/bg-2016-548, 2017
Manuscript under review for journal Biogeosciences
Published: 11 January 2017

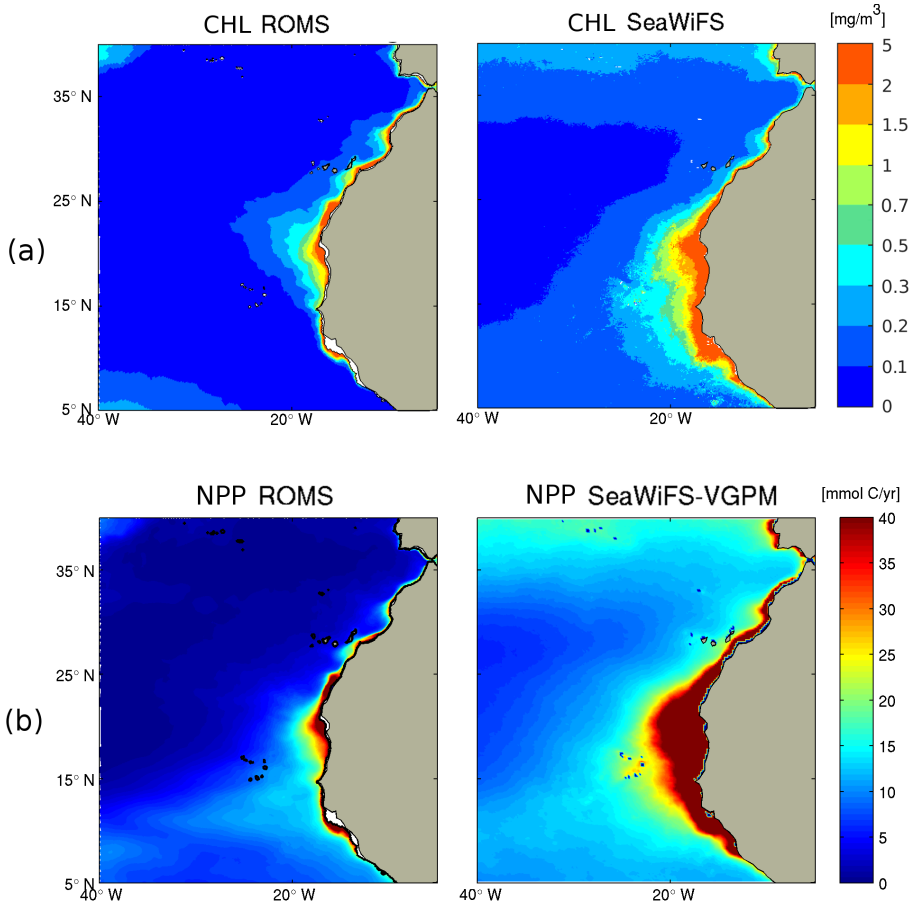

Figure 4. Maps evaluating the modeled chlorophyll and primary production in the CanUS. (a) Comparison of annual mean surface chlorophyll (CHL) between ROMS (left column) and SeaWiFS (right column). (b) Comparison of annual vertically integrated Net Primary Production (NPP) between ROMS (left column) and the VGPM estimate on the basis of the SeaWiFS data (right column). A detailed description of the data used for the evaluation is provided in Appendix A: Datasets, Table A3.

figures, Figure B2). The depth of the modeled CHL maximum is deeper than what can be expected for this region, according to local surveys. This deep bias of the chlorophyll maximum and therefore of production may be connected to the too deep modeled mixed layer in the surroundings of the Cape Verde Islands, a region in which the observed MLD is very shallow, or to a too fast depletion of the nutrients at the upper edge of the nutricline. This deeper than observed primary production may result in a less intense lateral transport of CHL in this subregion given the decline of the advective currents with depth. This potential limitation will be discussed in depth in throughout the paper.

Modeled vertically integrated chlorophyll (not shown) as well as total annual Net Primary Production (NPP) (Figure 4b), show instead intense biological activity in the southern CanUS, where NPP reaches values higher than in the northern subregion, especially offshore. However, modeled values of NPP are lower than the SeaWiFS VGPM estimates by about 3-fold.

Biogeosciences Discuss., doi:10.5194/bg-2016-548, 2017
Manuscript under review for journal Biogeosciences
Published: 11 January 2017

Other NPP estimates such as those based on SeaWiFS CbPM and Modis-Aqua VGPM provide substantially lower estimates of primary production that are slightly closer to our modeled values, but the comparison does not substantially change the picture (a detailed descriptions of all the used datasets is provided in Appendix A: Datasets, Table A3). Despite this underestimation, the pattern and the offshore gradient of the modeled NPP agree with the estimates and allow us to discuss the impact of the organic carbon fluxes in terms of relative changes in the local carbon availability. A nearly homogeneous 3-fold increase of the modeled NPP would in fact not affect this analysis, even though it would likely change the absolute values of the fluxes of organic carbon that may exceed those found by our study.

Modeled Particulate Organic Carbon (POC) concentrations have annual mean values between 5 mmolC/m^3 and over 20 mmolC/m^3 in the first 100m depth of the very productive shelf areas laying therefore in the range of in situ observations (Alonso-González et al., 2009; Arístegui et al., 2003; Santana-Falcón et al., 2016; Fischer et al., 2009). Concentrations decline in the offshore direction with a pattern similar to that of NPP and have maximum values located between 20 m depth in the shelf area and 70 m depth offshore. Due to the absence of sediment resuspension and of a mechanism of disaggregation of the large detrital particles in the model, deep peaks of POC such as those present in Alonso-González et al. (2009) are not observed in the annual mean modeled POC concentration; this limitation and its potential repercussion on the lateral organic carbon transport will be discussed in depth in the Discussion section.

A further important evaluation concerns the seasonal cycle, especially since the CanUS is characterized by the most intense seasonal variability among all EBUS (Chavez and Messié, 2009). The first 2 columns of Figure 5 show a comparison between model and observations of the seasonal variations of the circulation in the CanUS averaged in the first 15m, the depth of integration of the drifters. The plot reveals that the modeled CanUS circulation agrees well with the data collected by the drifters on the seasonal scale. As expected, an enhanced offshore flow is visible in summer in the northern Moroccan subregion and in winter and spring in the southern Mauritanian-Senegalese subregion. The alongshore Canary Current is clearly visible in the northern sector of the CanUS. The Mauritanian Current seems to be weaker than observed especially in summer and to a smaller extent in fall. However, the Mauritanian Current is clearly visible in Figure 3b, in which the simulated flow is vertically integrated over the first 100m depth. Vertical sections of the modeled meridional flow (not shown) also show a clear northward flow corresponding to the Mauritanian Current below 10m depth. The modeled Mauritanian current is therefore slightly deeper than observed, possibly due to a deeper MLD observed in the southern CanUS coast (see Figure 2). The seasonality of the Equatorial Counter Current (NECC) is well represented, even though its modeled flow in summer and fall is less intense than in the drifters data. The weaker than observed circulation in the southern sector of the CanUS will be taken into account in the discussion of the model results.

Since we are interested in quantifying the offshore fluxes of organic carbon throughout the upper few hundreds meters, vertically-integrated NPP is a better measure for evaluating the capacity of our model to reproduce the expected pattern of organic carbon than surface Chlorophyll. NPP in the CanUS is strongly influenced by the pattern of currents: the Cape Verde Frontal Zone separates a southern area of extended offshore production from a northern subregion characterized by a strong offshore decline in productivity (Arístegui et al., 2009). Both previous studies and SeaWiFS estimates show that productivity in the northern CanUS is dominated by a summer peak, while productivity in the southern CanUS shows a peaks in late winter

Biogeosciences Discuss., doi:10.5194/bg-2016-548, 2017
Manuscript under review for journal Biogeosciences
Published: 11 January 2017

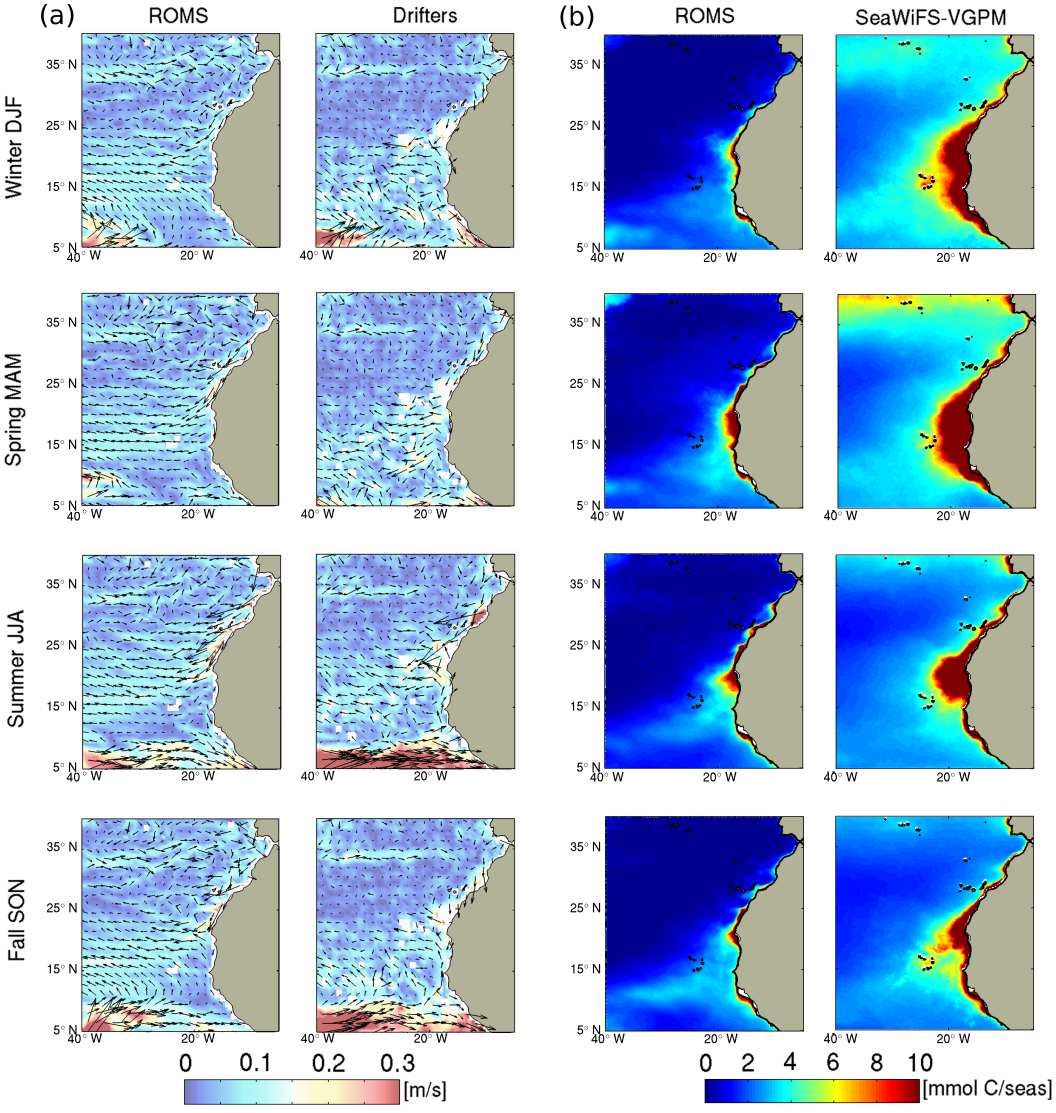

Figure 5. Subplot (a): Circulation in the EBUS by season. ROMS (left column) and drifters (right column), (Lumpkin and Johnson, 2013)]. ROMS output was integrated in the first 15m depth to be comparable with the drifters observations. Subplot (b): Vertically integrated Net Primary Production (NPP) from ROMS (right) and SeaWiFS VGPM estimate. A detailed description of the data used for the evaluation is provided in Appendix A: Datasets, Table A3.

and spring (Pelegrí et al., 2005). This seasonality and subregional variability is well represented by our model at all latitudes of the CanUS. In both model and observations, the southern Mauritanian-Senegalese subregion is the most productive area of the CanUS and is characterized by a reduced offshore gradient of NPP, while the northern Moroccan subregion is characterized by

Biogeosciences Discuss., doi:10.5194/bg-2016-548, 2017
Manuscript under review for journal Biogeosciences
Published: 11 January 2017

a sharp offshore gradient of production. The convergence of the coastal currents in the region of Cape Blanc fuels a persistent offshore bloom (Auger et al., 2016) that clearly appears both in the SeaWiFS product and in the model.

As visible from the Taylor Diagrams (Appendix B: Supplementary figures, Figure B3) the nice agreement between the pattern of the physical and biological variables of interest is also confirmed by the good correlation between modeled and observed fields both in the annual and in the seasonal means. The annual mean Taylor diagram shows values of correlation and relative standard deviation for MLD, SST and CHL comparable to those presented for the CanUS in the ROMS+NPZD study by Lachkar and Gruber (2011), despite the the boundaries of our grid being much further away, and therefore them providing much less contraints on the modeled physics and biology in the region of interest. When compared to similar studies using ROMS+NPZD in other upwelling systems such as the California Upwelling System (Gruber et al. (2011), whole domain), our Taylor diagram shows a slightly worse correlation and comparable standard deviation of surface CHL in the annual mean but a better seasonal representation, while modeled NPP has comparable performances.

4 Results

4.1 NCP: Linking sources and sinks of Organic Carbon

The simulation reveals in the long term mean a strong onshore-offshore difference in the vertically integrated NCP, i.e., primary production minus respiration/remineralization integrated from the bottom of the ocean up to the surface including remineralization in the sediments, i.e., $\int$NCP (Figure 6a).

The full water column $\int$NCP is negative across nearly the entire eastern subtropical North Atlantic, while only a narrow strip of less than 100 km along the north-western African coast and a few offshore regions in the southern part of the domain have positive values. This implies that the majority of the region is net heterotrophic, as within each column of water including the sediments more organic matter is being consumed than what is being produced locally. In contrast, the shelf regions of the CanUS are characterized by high levels of organic carbon production that exceed local consumption in the total water column and sediments, leading to a positive $\int$NCP and therefore an excess of organic carbon, which is available for lateral export.

A very different offshore gradient exists if NCP is just integrated over the top 100 m (Figure 6b). Despite the full water column heterotrophy of the offshore waters, the top 100 m of the CanUS have a positive NCP at every latitude and distance from the coast, i.e., are, on average, a net source of organic carbon. In contrast, NCP integrated from 100 m depth downward (Figure 6c) is everywhere negative, i.e., this part of the water column and the underlying sediments are net heterotrophic. Thus, the negative $\int$NCP of the offshore waters (Figure 6a) arises from the excess of respiration at depth over the net production in the overlying surface ocean.

This switch between positive and negative NCP in the CanUS happens on average at $\sim$60 m in the nearshore regions deepening to $\sim$100 m in the offshore region, separating a layer of high net production from a layer of intense net respiration (Figure 7a). This depth corresponds very closely to the euphotic zone depth, here defined by the level at which the light intensity at the surface is attenuated to 1%. Furthermore, this is also the depth of the maximum organic carbon concentration (Figure 7b). In the upper 100 m, the majority of this organic carbon stems from small detritus and phytoplankton, while below that

Biogeosciences Discuss., doi:10.5194/bg-2016-548, 2017
Manuscript under review for journal Biogeosciences
Published: 11 January 2017

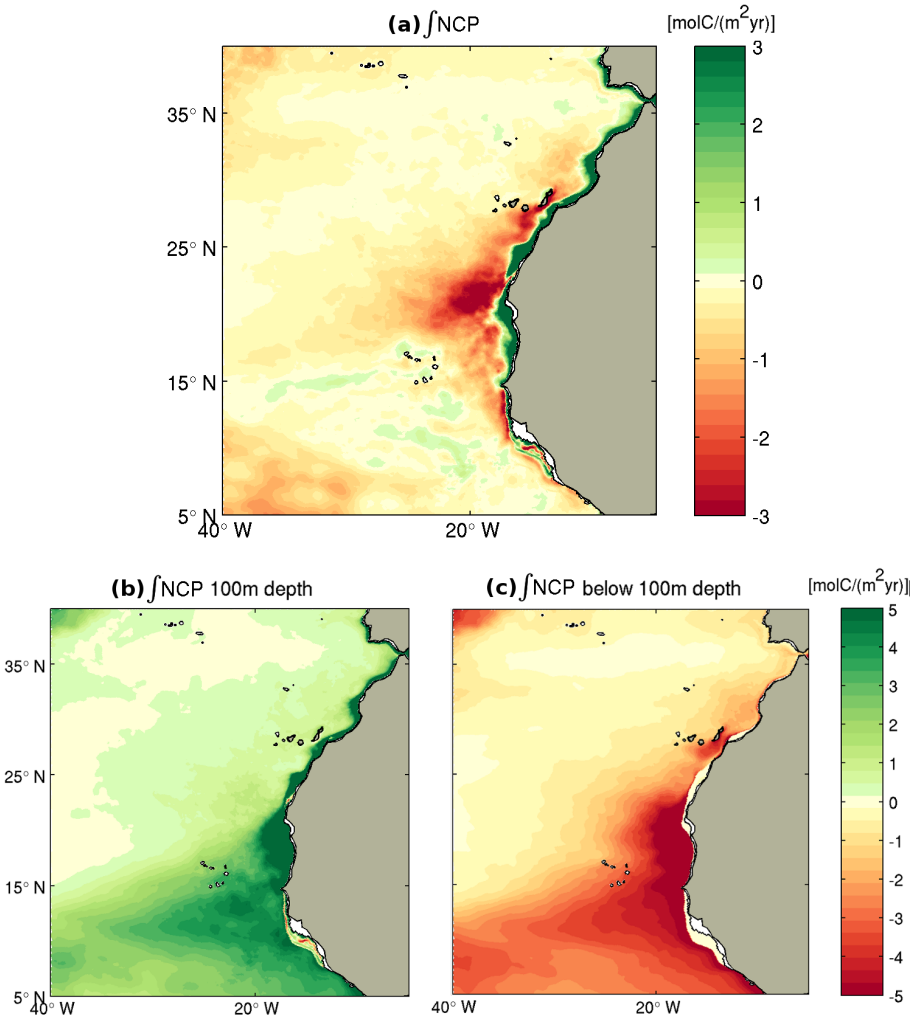

Figure 6. Maps of vertically integrated net community production. (a) NCP integrated over the full water column including sediment remineralization. This represents the net amount of organic carbon available for lateral redistribution. (b) NCP vertically integrated over the top 100 m only, including sediment remineralization. (c) As (b), for the depth range from 100 m to the bottom. Green indicates positive ∫NCP (net source of organic carbon) while red means negative ∫NCP (net sink of organic carbon).

depth and particularly in the nearshore areas, the large particles dominate. The contribution of zooplankton to the total organic carbon pool is substantial, but never dominant.

Since there is no accumulation of organic carbon in the long term mean in any of the reservoirs, this onshore-offshore gradient in ∫NCP requires a substantial amount of organic carbon that is transported from the shelf region into the open subtropical North Atlantic. To understand this complex spatial pattern of autotrophic and heterotrophic activity in the region we next quantify the lateral and vertical fluxes of organic carbon in the CanUS.

Biogeosciences Discuss., doi:10.5194/bg-2016-548, 2017
Manuscript under review for journal Biogeosciences
Published: 11 January 2017

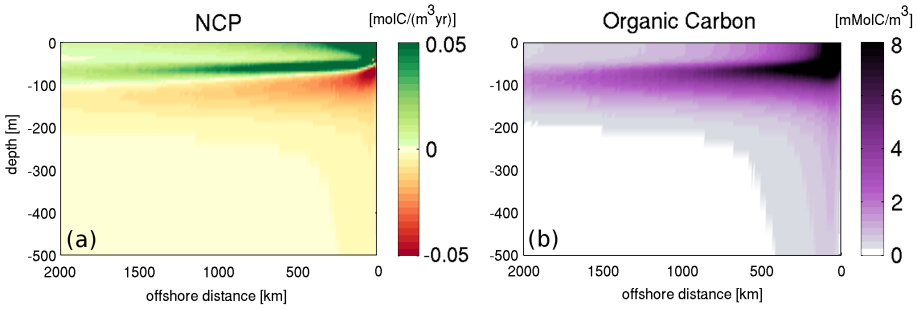

Figure 7. Mean vertical sections of (a) NCP and (b) organic carbon concentration in the Canary EBUS, averaged meridionally along lines of equal distance from the coast between 9.5°N and 32°N.

4.2 Long-range offshore transport of organic carbon

The dominant nature of the offshore transport of organic carbon from the northwestern African shelf becomes clear by inspecting the annual mean and meridionally averaged section of the zonal flux of organic carbon (Figure 8a). This transport is nearly everywhere negative, indicating a westward, i.e., offshore transport, with the exception of the very nearshore region, where the narrow upwelling cell recirculates the organic carbon back onshore. This offshore flux spans the entire 2000 km range of distances from the coast in the first 200 m of depth, resulting in a continuous displacement of the organic carbon from the nearshore waters to the open sea. Only in the very nearshore region, the narrow upwelling cell causes the zonal flux to recirculate the organic carbon onshore.

In the vertical direction, the intensity of the offshore flux is maximum at the surface, and generally decreases with depth, except for the offshore regions, where a secondary maximum of zonal offshore transport occurs at around 100 m. Below that depth, the transport decreases rapidly and tapers off to very low values below 200 m with the exception of first 500 km from the coast. While the surface maximum of the offshore flux is mainly driven by the intense mean zonal velocity, the intensification of the flux around 100 m in the offshore waters is strongly influenced by the pattern of the organic carbon concentration (Figure 7b).

The lateral meridional flux (Figure 8b) is weaker than the zonal flux and going downward and offshore has a complex alternation of northward and southward fluxes. In particular, the intense southward flowing Canary Current results in a negative signature of the mean meridional flux near the coast, while northward fluxes, probably linked to an influx from the organic carbon-rich near equatorial region, are dominant offshore.

The vertical advective and mixing (eddy-diffusive) fluxes (Figure 8c) are overall much weaker than the vertical sinking flux (Figure 8d). The latter, as expected from the fact that we employ constant sinking speeds has a pattern that reflects directly that of the organic carbon concentration (Figure 7b). In contrast, the fact that the vertical advective and mixing fluxes depend on the mean circulation results in a more complex pattern. These fluxes are positive both near the coast in response to the strong upwelling and in the upper first tens of meters where the vertical mixing redistributes the organic carbon against its vertical

Biogeosciences Discuss., doi:10.5194/bg-2016-548, 2017
Manuscript under review for journal Biogeosciences
Published: 11 January 2017

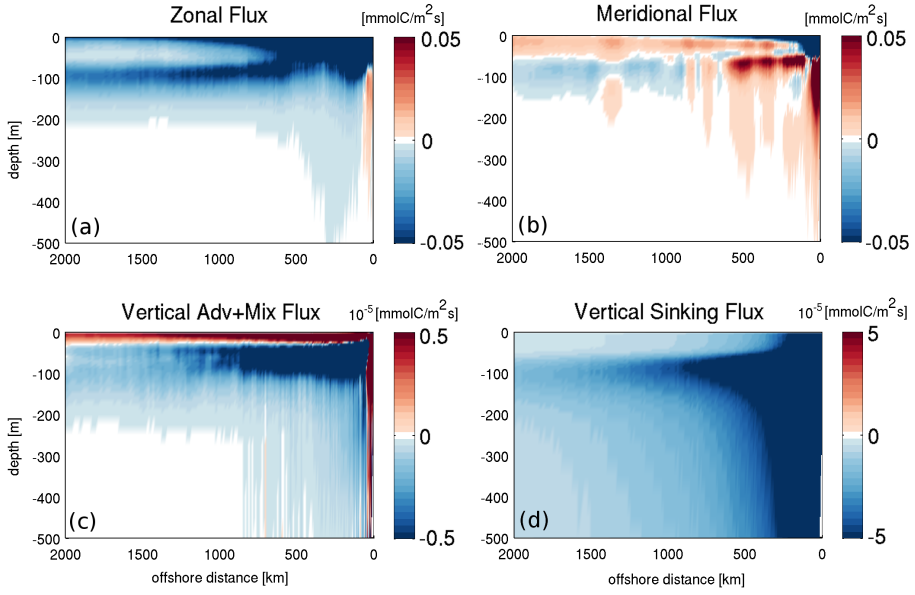

Figure 8. Mean vertical sections of the physical fluxes of organic carbon in the Canary EBUS, averaged meridionally along lines of equal distance from the coast between 9.5°N and 32°N. (a) Zonal flux of organic carbon with positive values indicating eastward (onshore) transport. (b) Meridional flux of organic carbon with positive values indicating northward transport. (c) Sum of vertical advective and mixing (eddy-diffusive) fluxes with positive values meaning upward transport. (d) Vertical sinking flux with negative values indicating downward transport.

gradient. Below this shallow layer, subduction and downward mixing are dominant and contribute to the export of organic carbon to depth.

Reflecting the relative contribution of the different pools to the total organic carbon, the fluxes below the first 200 m as well as the vertical sinking flux are dominated by the contribution of the large detritus that reaches deep into the water column declining in concentration in the offshore direction. In the first 200 m, abundant small detritus, phytoplankton and to a smaller extent zooplankton shape the organic carbon fluxes up to the farthest boundary of the analysis domain.

4.3 The organic carbon budget

The annual mean budget for organic carbon for the upper waters of the whole CanUS highlights the key contribution of the offshore flux to the enhancement of the organic carbon pool and the maintenance of the heterotrophic activity in the open waters (Figure 9a and Figure 10a). In the upper 100 m corresponding roughly to the euphotic layer, the offshore flux is the dominant lateral flux at all distances with a magnitude that always exceeds 10 % of the integrated NCP within the box (Figure 9a). More specifically, at 100 km from the coast the offshore flux of organic carbon transports as much as 1.6 Tmol C yr^{-1} (18.7 Tg C yr^{-1}), a quantity that amounts to more than a third of the integrated NCP in the 0 km-100 km range, i.e. the first coastal box, and to 18 % of the Net Primary Production, NPP_{100km} = 8.6 TmolC yr^{-1}.

Biogeosciences Discuss., doi:10.5194/bg-2016-548, 2017
Manuscript under review for journal Biogeosciences
Published: 11 January 2017

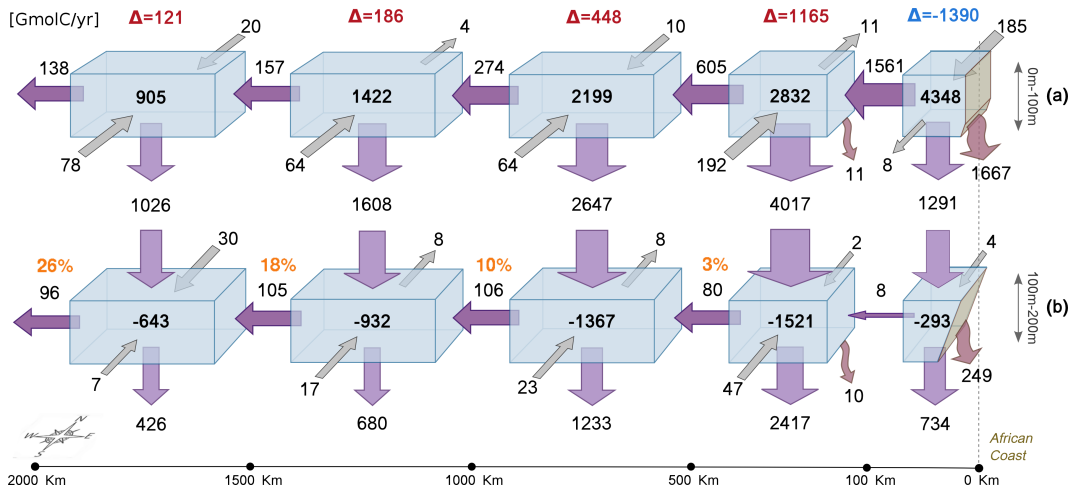

Figure 9. Annual mean Organic carbon budget for CanUS as a whole in units of GmolC yr^{-1} for (a) the top 100 m, and (b) for the 100 m-200 m depth range. The lateral extension of the budget analysis boxes is shown in Figure 3b. The African coast is located on the right edge of the x-axis, with the offshore distance indicated at the bottom. Numbers inside the boxes represent the net biological flux in the volume (integrated NCP). The Arrows between boxes represent physical fluxes with the dimension of the arrows being scaled according to the magnitude of the fluxes. Lateral fluxes are advective, vertical fluxes are divided into fluxes between boxes (straight arrows, advective+mixing+sinking) and sinking fluxes to the sediments (bent arrows). The symbol Δ = Vertical Export - NCP in (a) is a measure of the excess vertical export in each box with $\Delta > 0$ indicating that the vertical export exceeds local NCP. The orange percentages in (b) represent the fraction of non-respired influx from above that is exported offshore.

A good measure for the magnitude and impact of the lateral redistribution of organic carbon is the difference between the organic carbon that is produced locally through NCP, and the amount of organic carbon that is exported vertically out of the euphotic zone (here taken as the 100 m). In the absence of any lateral redistribution, this difference, termed excess export, i.e., ΔE = Vertical Export - NCP is zero, while in the case of a strong lateral export of the organic matter, ΔE is negative since less carbon is available for the vertical export at depth. Conversely, if a particular region is importing a large amount of organic carbon through lateral transport and then exporting this carbon to depth, then the excess export ΔE is positive.

The analysis of ΔE as a function of offshore distance reveals that all regions have a positive ΔE with the exception of the nearshore one, whose ΔE is instead negative (Figure 9a). Thus, this supports the notion that the net heterotrophic activity over the whole water column in the offshore direction is fueled by a strong net growth in the very nearshore region of the CanUS. The magnitude of excess export at depth ranges between 41 % of NCP in the 100 km-500 km range to 13 % of NCP in the most distant region (orange solid line of Figure 10a) accounting for hundreds to thousands of Gmol of organic carbon per year. This excess export of organic carbon below 100m is explained by the divergence of the lateral fluxes. This divergence releases in each region an amount of organic carbon that constitutes between 8 % and 34 % of the local NCP, with the highest value in the 100 km-500 km offshore range, and explains with this organic carbon accumulation from 62 % to 80 % of the excess export at depth in the first 1500km offshore (Figure 10a, purple solid line). In the most distant analysis region (1500 km-2000

Biogeosciences Discuss., doi:10.5194/bg-2016-548, 2017
Manuscript under review for journal Biogeosciences
Published: 11 January 2017

km range) the offshore flux divergence drops, resulting in a significant export of organic carbon through the 2000 km offshore boundary and little accumulation; this flux may impact the biological activity even farther in the North Atlantic Gyre.

The alongshore (N-S) lateral fluxes also positively contribute to the total budget with a net influx of organic carbon in the euphotic layer (Figure 9a). However, the divergence of the alongshore flux exceeds 10 % of the local NCP only in the most distant analysis region (blue solid line of Figure 10a) and represents therefore a minor contribute to the excess export at depth.

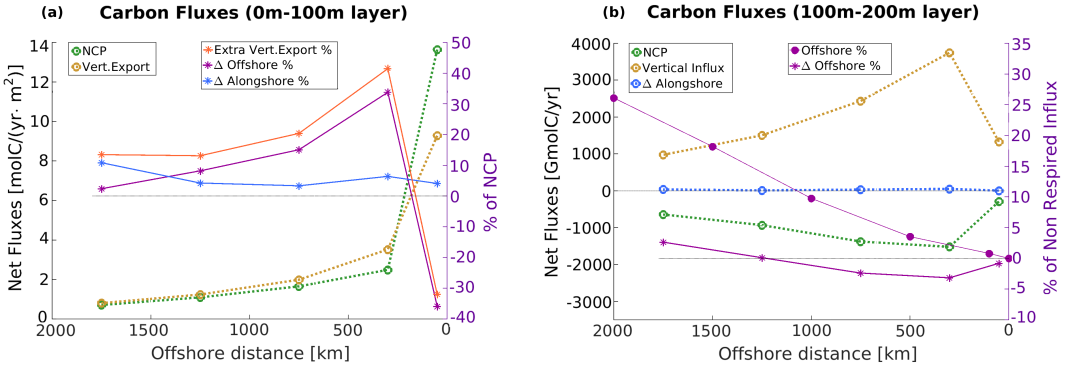

Figure 10. Main flux trends in the CanUS as a function of offshore distance for (a) the top 100 m and (b) for the 100 m-200 m depth range. In both panels: dotted lines refer to the left y-axis, solid lines refer to the right y-axis. Quantities represented by solid lines are expressed as percent of the significant carbon source for the layer, respectively: NCP for the top 100 m in (a), and the non-respired influx of carbon for the 100 m-200 m depth layer in (b). Δ fluxes represent the divergence of the fluxes: net amount of carbon accumulated or removed by the flux in each box. All net fluxes are binned at the center of the box of reference (e.g., fluxes in the 0 km-100 km region are binned to 50 km offshore), except for the offshore flux in panel (b), which refers to the boundaries of the boxes. Note that in panel a, the vertical export is a negative flux and that the yellow dotted line refers to its magnitude, and that ΔE is the excess vertical export as in Figure 9a). In panel b, the non respired influx is computed by summing the vertical influx, the alongshore flux, and NCP.

The fate of the vertically exported carbon in the very biologically active 100 m-200 m depth layer is still strongly influenced by the offshore transport (Figure 9b), except for the nearshore, where the upwelling cell recirculates the organic carbon onshore. The offshore flux intensifies moving away from the coast, reaching its maximum at 1500 km distance from the coast, where its intensity becomes comparable to that of the top 100 m. Given the negative contribution of NCP to the organic carbon budget in this layer, the magnitude and divergence of the offshore flux at this depth can be compared to the non-respired influx of organic carbon, i.e., the amount of incoming carbon that is available in each box after remineralization. The main sources of organic carbon at this depths are the incoming vertical flux from the euphotic layer and to a very small extent the divergence of the lateral alongshore flux (respectively yellow and blue dotted lines of Figure 10b). Therefore, the non-respired influx is defined as the sum of the incoming vertical flux, the divergence of the alongshore flux and the negative NCP.

If we compare the offshore flux at the boundary of the boxes to the non-respired influx in each box we see that the offshore flux moves a substantial amount of the organic carbon available, reaching 26% at 2000 km distance from the shore (purple solid line with circles of Figure 10b). At the same time, due to its intensification in the direction of the open sea, the offshore

Biogeosciences Discuss., doi:10.5194/bg-2016-548, 2017
Manuscript under review for journal Biogeosciences
Published: 11 January 2017

flux does not release carbon in the boxes as confirmed by its negative divergence up to 1500km offshore distance (purple solid line with stars of Figure 10b and percentages in orange in Figure 9b), but it traps it and transports it even farther toward the open waters. The 100 m-200 m depth layer of the CanUS is therefore still characterized by a significant offshore transport that moves the organic carbon towards the oligotrophic center of the North Atlantic Gyre, furthering water column heterotrophy there.

As the offshore fluxes are small below 200 m (Figure 8a), we omitted them from the plot. In fact, the maximum contribution to the total offshore transport of the water column below 200 m, accounting for a few kilometers of depth, is 12 % reached at 500 km of distance from the shore. This fraction quickly declines offshore to a minimum of only 0.4 % at 2000 km of distance from the shore. Thus, the vast majority of the transport occurs in the top 200 m of the water column in our model.

4.4 Subregional variability of the organic carbon fluxes

Substantial zonal differences in both biological activity and circulation characterize the CanUS and influence the pattern of the organic carbon fluxes. Latitudinal gradients in net primary production and in the distribution of sources and sinks of organic carbon emerge from the plot of vertically integrated NCP (Figure 6). In its northern portion, the CanUS is characterized by a weak offshore gradient of deep respiration and a sharp offshore gradient of production in the euphotic layer, resulting in an extended net water column heterotrophy in the open waters. In contrast, the southern CanUS is characterized by a widespread vertical correspondence between shallow sources and deep sinks of organic carbon that result in a nearly neutral water column ($\int$NCP$\sim$ 0), with negative values of $\int$NCP confined only between the African shelf and the Cape Verde archipelago. Between these two zonal bands with distinct $\int$NCP signatures, the central surroundings of Cape Blanc (21°N) and the whole Cape Verde frontal zone are hot-spots for the respiration of the organic carbon. Here, the region of deep intense remineralization extends farther offshore than the area of near-surface productivity, resulting in a vast peak of negative $\int$NCP that reaches far into the North Atlantic Gyre. To identify what processes drive the organic carbon redistribution that give rise to these $\int$NCP gradients and quantify the contribute of the different zonal bands to the total transport we analyze in detail the spatial patterns of the physical fluxes of organic carbon.

Subregional differences in the organic carbon transport are visible in all of the components of the physical fluxes (Figure 11). Both zonal and meridional fluxes integrated over the top 100 m are clearly influenced by the regional pattern of currents (see also Figure 3b) and change sign in the proximity of the Cape Verde frontal zone, the crucial boundary between the northern anticyclonic and the southern cyclonic circulation. Above the Cape Verde front, the zonal flux is mostly offshore and intensifies moving towards Cape Blanc likely due to both the intense coastal mesoscale activity that culminates at 21°N with the giant Cape Blanc filament and to the formation of the Cape Verde front. South of Cape Blanc, ocean striations appear in the form of alternate onshore and offshore flux bands. The meridional transport converges around Cape Blanc, again with a sharp inversion of sign that reflects the direction of flow of the Canary Current and the Mauritanian Current.

The 100 m horizontal section of the vertical advective transport of organic carbon reflects the signature of the wind stress curl that is negative north the Cape Verde front and positive to the south. As a consequence, the highest values of advective export at depth are found in the northern regions of low offshore production, while vertical advective export of organic carbon

Biogeosciences Discuss., doi:10.5194/bg-2016-548, 2017
Manuscript under review for journal Biogeosciences
Published: 11 January 2017

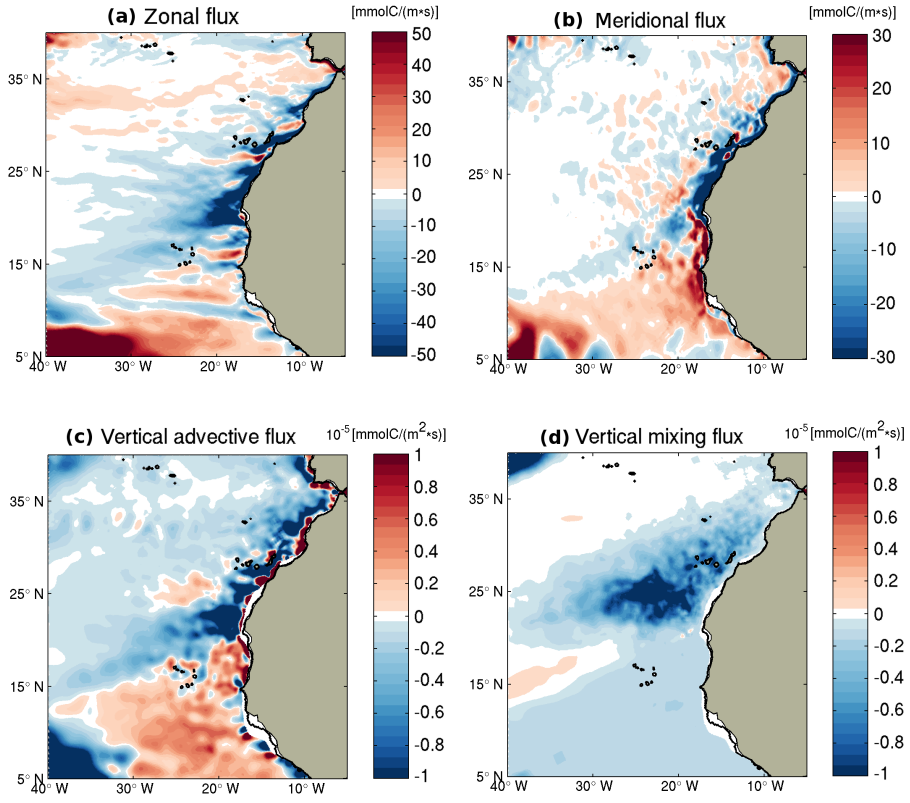

Figure 11. Maps of the organic carbon flux components in the top 100 m corresponding roughly to the euphotic layer in the CanUS. (a) Zonal flux vertically integrated over the top 100 m with positive values indicating eastward (onshore) transport. (b) as (a), but for the meridional flux with positive values indicating northward transport. (c) vertical advective flux across 100 m with positive values indicating upward transport. (d) as(c) but for vertical mixing. Plotted vertical components were smoothed with a 7x7 grid points 2-dimensional filter.

is not favored in the very productive southern subregion. As for the offshore transport, also the vertical advective export in the northern CanUS sector and on the Cape Verde frontal zone is likely enhanced in the first few hundreds of kilometers by the abundant coastal filaments that quickly channel and downwell the coastally produced organic carbon. The vertical mixing fluxes of organic carbon across 100 m shows that this component is important only in the northern subregion characterized by a much deeper MLD, and declines offshore with the decrease of the organic carbon concentration. Sinking fluxes through the 100m depth are not shown as their pattern is mostly proportional to the 100m-integrated NCP (Figure 6b) with high export in regions of high production and do not add substantial complexity to the discussion. However, it is worth remarking that their intensity is about one order of magnitude higher than that of the vertical advective and vertical mixing fluxes, reaching very intense peaks (∼-40 molC/(m^{2}day)) in the surroundings of the most productive region of Cape Blanc, and high values of about -10 molC/(m^{2}day) in the Mauritanian-Senegalese subregion. The southern sector of the CanUS is therefore dominated

Biogeosciences Discuss., doi:10.5194/bg-2016-548, 2017
Manuscript under review for journal Biogeosciences
Published: 11 January 2017

by intense sinking fluxes of organic carbon, while both non-sinking vertical components of the export have a very limited role in the organic carbon export in the region below Cape Blanc.

The analysis of the spatial pattern of the organic carbon fluxes also remarks the special role of the central zonal band located between the Canary Archipelago and the Cape Verde Islands, characterized by the most intense biological and physical fluxes. This central zonal band is characterized by the strongest heterotrophic activity offshore, a persistent and intense offshore transport, a convergence of the lateral alongshore fluxes in the shelf, strong vertical advective export at depth, intense vertical mixing and a peak of the sinking flux. To highlight how differently the physical fluxes impact the organic carbon budget at different latitudes and to study the interaction between significant zonal bands in the CanUS we divided the region into southern, central and northern subregions (defined as in Figure 3b) and carried out a subregional box budget analysis.

Among the CanUS subregions, the Southern subregion (pink line of Figure 12) is characterized by very high levels of NCP in the euphotic layer also in the open waters (Figure 12a) accompanied by a relatively low impact of the physical fluxes of carbon on the local budget. In fact, despite both the offshore transport and the vertical advective+mixing export below 100 m have high intensities in absolute terms, their divergences are low when compared to the high values NCP in each box and therefore they do not have a substantial impact on biology (Figure 12b and Figure 12d). On the one side, the little accumulation of organic carbon due to the offshore flux explains the large portion of biologically neutral water column in this region ($\int$NCP$\sim$0, see Figure 6a). On the other side, even though the sinking fluxes (Figure 12e) still export substantial amounts of carbon in this subregion, the low efficiency of advective+mixing export points to a potentially limited capacity of this subregion to export at depth dissolved and suspended material (not modeled in our study). The comparatively higher impact of the alongshore flux is explained by the strong coupling of the southern subregion with the equatorial carbon rich area that allows a net influx of organic carbon through the southern boundary.

The impact of the lateral offshore transport in the Northern subregion (blue line of Figure 12) is particularly high in the first 500 km offshore (Figure 12b). This is the result of a combination of both strong export fluxes on the shelf and of the fast decline of NCP in the offshore direction, with a consequent high ratio of the offshore flux divergence to NCP and an important influence of the flux on the local budget. The intense mesoscale activity in this northern subregion, especially in the form of persistent filaments that detach from the coast and quickly channell water and tracers offshore typically for some hundreds km, has an important role in this intense nearshore export. The northern subregion is also the most efficient in the vertical advective+mixing export up to 1000 km offshore as a consequence of the deep MLD and the abundant mesoscale coastal filaments, with a consequently high capacity to export light organic carbon species below the euphotic layer. However, both lateral and vertical export efficiency decline quickly moving offshore in the northern subregion. This decline is likely due to the low organic carbon concentration of the offshore waters, to the limited offshore extension of the filaments and to the incoming flux of the Azores Current counteracting the offshore transport at the northern edge of the domain.

As anticipated, the most active area in terms of organic carbon transport and export is the central CanUS subregion (green line of Figure 12, which includes the Cape Verde frontal zone. The central subregion collects the lateral alongshore fluxes from the northern and southern subregions in the nearshore area, with a net increase of the carbon availability in the first coastal box (0 km-100 km range) of more than 1/3 of the local NCP (Figure 12c). The southward flowing Canary Current

Biogeosciences Discuss., doi:10.5194/bg-2016-548, 2017
Manuscript under review for journal Biogeosciences
Published: 11 January 2017

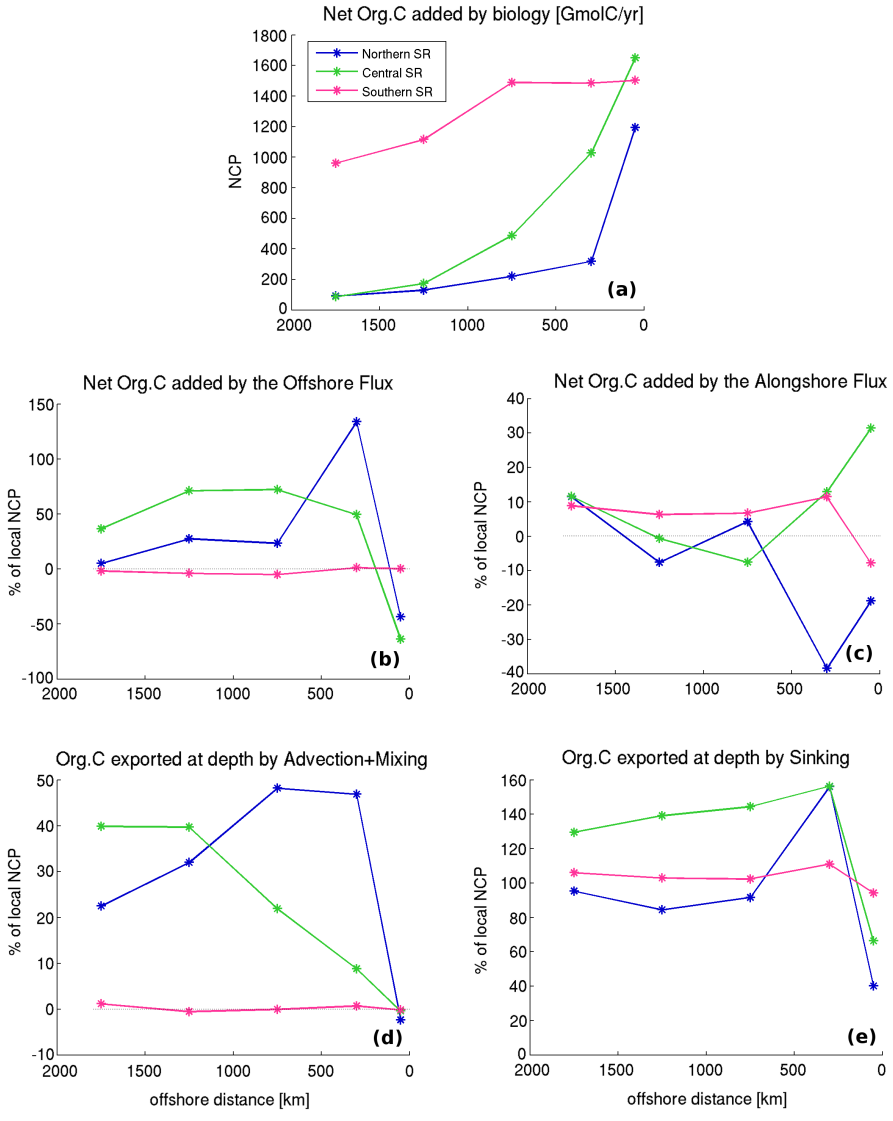

Figure 12. Trends of NCP and impact of the organic carbon fluxes (divergence of the flux / NCP) by subregion and offshore distance in top 100 m as a function of offshore distance. (a) XXX ADD description Fluxes in the plots are binned at the center of the box of reference (eg, fluxes referring to the 0 km-100 km box are binned to 50 km offshore on the x-axis). NCP is integrated through the whole volume of each box. Flux impacts, i.e., the net amount of organic carbon added in each box by the divergence of the flux, are expressed in percent of the local NCP.

and northward flowing Mauritanian Current that converge in this zonal band are the main contributors to this organic carbon influx on the coast around Cape Blanc. The carbon collected on the shelf is likely exported offshore together with the locally produced carbon by a very intense zonal flux characterized also by a large divergence that exceeds the values of the northern

Biogeosciences Discuss., doi:10.5194/bg-2016-548, 2017
Manuscript under review for journal Biogeosciences
Published: 11 January 2017

subregion in the offshore waters (Figure 12b). The carbon accumulation due to the divergence of the offshore transport over the central zonal band is on average as high as 57 % of the local NCP, reaching peaks of more than 70 % of NCP in the 500 km-1500 km range and still accounting for 37 % of NCP in the farthest offshore box (1500 km-2000 km range). Both the mean circulation characterized by the westward flowing currents along the Cape Verde front and the mesoscale activity in the form of the giant Cape Blanc filament are expected to contribute to this intense offshore transport. As a consequence of this increased carbon availability, the central subregion allows very high values of the total vertical export of carbon below the euphotic layer (advective+mixing+sinking transport), which almost doubles the local production. Among these vertical components, the advective+mixing vertical export becomes particularly important the offshore waters. The alongshore convergence of organic carbon on the shelf and the high lateral mobility of the organic carbon in the offshore direction of the central subregion not only explain the peak of net water column heterotrophy in the offshore waters around Cape Blanc (see Figure 6a), but they characterize the Cape Verde frontal zone as a key region of the CanUS for the collection and export of the coastally produced organic carbon far into the North Atlantic Gyre.

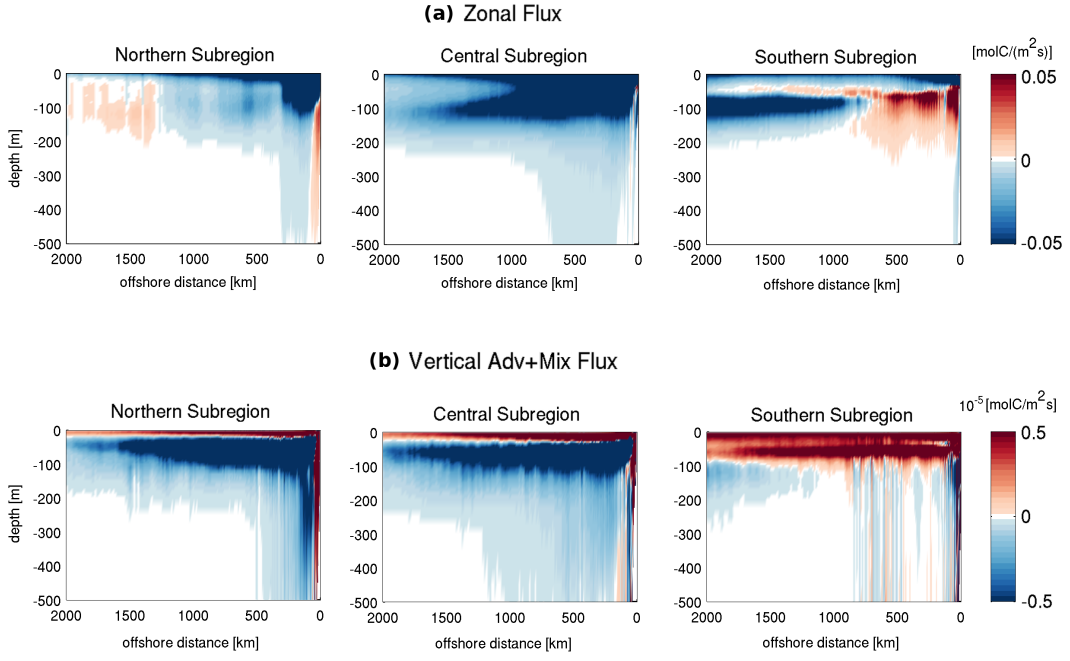

Figure 13. Vertical sections of the organic carbon offshore flux (a) and vertical advective+mixing flux (b), averaged meridionally along lines of equal distance from the coast in each subregion in accordance to the zonal bands defined by the budget analysis boxes. In all the plots the horizontal x-axis represents the distance from the coast (km); the vertcal y-axis represents the depth (m). Subplot (a) Zonal flux: positive means eastward (onshore); Subplot (b) Vertical advective + mixing (eddy-diffusive) flux: positive means upward.

Further insights in the zonal differences of the organic carbon transport below the euphotic layer are given by the zonally averaged mean vertical profiles of the offshore and vertical advective+mixing fluxes for each subregion (Figure 13. The south-

Biogeosciences Discuss., doi:10.5194/bg-2016-548, 2017
Manuscript under review for journal Biogeosciences
Published: 11 January 2017

ern subregion is confirmed to be the least efficient in the offshore transport and vertical advective+mixing export also at depth, despite an intensification of the offshore flux below the surface in the farthest region of analysis. This offshore intensification is however probably connected to the intersection of our southern zonal band with the Cape Verde frontal region which crosses the northern boundary of this subregion at about 1000 km offshore. The vertical advective+mixing export in the southern subregion is also remarkably different from the other subregions: not only the shallow MLD limits vertical mixing but the positive signature of the wind stress curl favors upwelling in this subregion. The mean vertical profiles of the zonal flux for the northern subregion shows clearly in the offshore waters below the surface a weak onshore flux that confirms the important influence of the incoming Azores current in the limitation of the offshore transport away from the coast. The deep extension of both the offshore flux and of the vertical advective+mixing downwelling in the first few kilometers from the coast of the northern subregion suggests again the link with the recurrent coastal filaments that characterize this sector of the CanUS and are known to enhance the fluxes through a depth of several hundreds of meters. The central subregion presents also at depth the most intense and persistent offshore flux that reaches 2000 km from the coast in the whole first 200 m layer, remarking the important role of this subregion for the offshore redistribution of the organic carbon. Both offshore and advective+mixing fluxes extend particularly deep into the water column in the first several hundreds of kilometers from the coast in the central subregion, likely due to both the intense mean circulation and the powerful giant Cape Blanc filament renown for its remarkable offshore extension. In both the northern and central subregions the offshore gradient of the zonal flux is the cause of the important accumulation of organic carbon that allows an enhanced respiration at depth.

The results of our subregional analysis show how physical forcing, mean and mesoscale circulation drive the lateral and vertical redistribution of the organic carbon in the CanUS, giving rise to a persistent offshore transport of organic carbon that shape the $\int$NCP pattern and can reach as far as 2000 km into the North Atlantic Gyre.

5 Discussion

The results of our modeling study highlight the importance of the lateral transport of organic carbon from coastal regions of intense production to the oligotrophic open waters and its key role in fueling the offshore heterotrophic activity, confirming the predictions of several in situ observations and estimates from multiple independent local surveys (Arístegui et al., 2009; Pelegrí et al., 2005). With our study we provide a detailed quantification of the total lateral transport in the whole CanUS and of its long-range influence.

The modeled offshore transport of coastal production lies in the range of previous estimates (Duarte and Cebrián, 1996), with about 18 % of the phytoplankton NPP (36% of NCP) being exported from the shelf to the open sea across the 100km distance line from the coast. Our results reveal also that the offshore transport does not decline to zero in the open ocean, where it still has important consequences for the biological activity: the enhancement of the carbon availability due to the offshore influx can still be as big as 37% of the local net community production between 1500 km and 2000 km offshore. The offshore transport is relevant also below the euphotic layer, especially in the 100m-200m layer, allowing the lateral transport of the sunk or downwelled organic carbon and reaching far into the North Atlantic gyre.

Biogeosciences Discuss., doi:10.5194/bg-2016-548, 2017
Manuscript under review for journal Biogeosciences
Published: 11 January 2017

The offshore transport below 200 m is generally very small, and never larger than 12 % of the total transport. However, model limitations in the representation of the offshore transport at depths below the first few hundreds meters should be discussed taking into account three potential and partially contrasting caveats. First, the model does not include the process of sediment resuspension, therefore impeding the formation of deep spots of high POC concentration near the shelves (Inthorn et al., 2006a; Alonso-González et al., 2009) and limiting the bottom transport along the slopes (Inthorn et al., 2006b; Hwang et al., 2008). Second, and with a similar effect, the dynamics of our particulate pools only allows the aggregation of small particles into bigger and heavier ones, while it does not allow disaggregation of heavy particles into lighter ones as a consequence of degradation or partial grazing (Alonso-González et al., 2010), resulting in a one-way path to fast sinking that cannot be reversed. Due to these two factors that preclude the existence of deep maxima of suspended POC, our study may underestimate the lateral transport of organic carbon at depth. Third, sinking velocities in our model are fixed at every depth to relatively small values (maximum of 10 m day^{-1} for large detritus), while sinking velocities have been observed to be able to reach relatively high values, increasing by roughly an order of magnitude between the mesopelagic and bathypelagic regions (Fischer and Karakaş, 2009; Berelson, 2002) with a consequent fast vertical export at depth of the particles by sinking. Heavy particles at depths below 1000 m have been shown to have mean sinking velocities of 100-300 m day^{-1} (Fischer and Karakaş, 2009) and to be often accompanied by a pool of slow sinking material with mean sinking velocities of 1 to a few m day^{-1}, resulting in a bimodal distribution of the sinking speeds (Alonso-González et al., 2010). Viewing these three caveats together, we have two missing processes that would cause the correct offshore transport to be larger than modeled, and one process that would cause the correct offshore transport to be smaller. We cannot assess the implication of this finding in full, but submit that at least with regard to the offshore transport in the upper waters, i.e., upper 200 m, our model is likely in the right range. We have much less confidence in the offshore transport below 200 m, where the observed concentrations of organic carbon can be quite high, although the offshore velocities are substantially smaller.

The total long-range offshore transport that reaches in our model as far as 2000 km from the coast in the central subregion can be explained by two possible schemes of interplay of biological and physical fluxes. In a first hypothesis, the offshore transport is sustained entirely by the excess organic carbon produced on the African shelf, which gets advected offshore up to the final boundary of our analysis domain getting only partially remineralized and exported at depth along the way. In a second hypothesis, the offshore flux of organic carbon is sustained by the production of organic carbon that happens along the way to the open sea: new and regenerated offshore production substitutes the incoming coastal organic carbon that gets remineralized and sinks at depth in a continuous rejuvenation of the organic carbon that is advected offshore. This offshore production would be sustained by nutrients either upwelled near the coast and advected offshore or by nutrients obtained from the local remineralization of the incoming carbon. The vertical pumping of the nutrients from the deeper waters offshore would be significant only in regions of positive wind stress curl (in our case only the southern CanUS) or abundant in mesoscale eddies. A simple analysis of the residence times of the modeled organic carbon pools makes us inclined to sustain the second hypothesis. In fact, a small detritus particle would likely reside in the first 200 m depth layer on average about 200 days due to its sinking speed if we disregard advective and mixing downwelling; given typical lateral velocities of less than 0.05 m/s when averaged through 200 m depth, this particle would be able to travel at best about 800km offshore. This distance must be

Biogeosciences Discuss., doi:10.5194/bg-2016-548, 2017
Manuscript under review for journal Biogeosciences
Published: 11 January 2017

divided by 10 in the case of large detritus and doubled in the case of phytoplankton, making it very unlikely for the coastally produced organic carbon to reach as far as 2000 km in the open sea. Even though zooplankton is the only organic carbon species that doesn't sink in the model, its modest contribution to the offshore fluxes, compared to those of phytoplankton and of the abundant small detritus, cannot justify the magnitude of the observed lateral transport. Further analysis such as Lagrangian experiments coupled with the biological fluxes are necessary to gain a quantitative understanding of the succession of transformations happening along the way to the open waters.

Meridional alongshore transport also contributes to the organic carbon redistribution, especially on the shelf region where we find the maximum intensity of the coastal currents. In line with the results of Auger et al. (2016) we find that the area around Cape Blanc, corresponding to the region of convergence of the coastal flows and formation of the Cape Verde frontal zone, is a key region of the CanUS. The relevance of the central Cape Verde frontal zone in the CanUS was discussed in Auger et al. (2016) in terms of chlorophyll and nutrient convergence on the shelf and of their subsequent offshore advection, visible as a persistent bloom in correspondence of the Cape Blanc region. Here we confirm and strengthen this observations, affirming that this sector of the CanUS has a central role in collecting on the shelf and then transporting offshore coastally produced organic carbon, allowing intense water column heterotrophy at depth in its proximity. This offshore flux of carbon against the gradient of productivity extends far away from the coast and feeds the heterotrophic activity of the deep open waters for at least 2000 km of kilometers offshore, generating a long tail of net heterotrophy. Deep offshore transport and subduction in this region are likely enhanced by the persistent giant Cape Blanc filament, which is known from local surveys for being able to transport an estimated 50 % of the coastally produced carbon both in the surface and at depth, reaching an extension of several hundreds of km offshore (Gabric et al., 1993; Ohde et al., 2015).

The natural partition of the CanUS into a northern anticyclonic and a southern cyclonic circulation and the subregional differences in both mesoscale activity and wind stress curl (Arístegui et al., 2009) are reflected into differences in the transport and cycling of the organic carbon north and south of the Cape Verde frontal zone. The northern CanUS located above the Cape Verde frontal zone can be regarded as the very eastern edge of the North Atlantic Gyre (Pelegrí et al., 2005), which receives from the shelf of this CanUS sector a relevant amount of organic carbon. Several studies highlight the way in which the abundant coastal filaments of this northern CanUS sector substantially enhance the offshore transport and the downwelling of organic carbon in the first hundreds of kilometers from the coast (Álvarez Salgado et al., 2007; Gabric et al., 1993; Fischer et al., 2009; García-Muñoz et al., 2005; Ohde et al., 2015). These structures together with a strong mean offshore flow explain the intense modeled zonal transport and vertical downwelling in the shelf region of the northern CanUS and their sharp decline in the open waters. The range of influence of the offshore transport in this zonal band may be further enhanced by multiple eddies spun by the filaments (Barton et al., 2004), while the negative signature of the wind stress curl maintains the vertical downwelling dominant also offshore. Our model overestimates the MLD depth and therefore potentially the mixing export at depth in this region (see section 3. Evaluation); however the observed MLD pattern still presents a strong meridional gradient with an extremely shallow mixed layer in the southern region below the Cape Verde front and deeper mixed layer in the north, favoring intense mixing. The strength of both the mixing and the advective vertical transport indicate that the northern subregion is potentially efficient in exporting at depth the dissolved, suspended and slowly settling material, organic carbon

Biogeosciences Discuss., doi:10.5194/bg-2016-548, 2017
Manuscript under review for journal Biogeosciences
Published: 11 January 2017

species that are also difficult if not impossible to measure with sediment traps but may still constitute the key component for the closure of the organic carbon budget at depth (Hopkinson and Vallino, 2005; Alonso-González et al., 2010).

The southern CanUS sector, located below the Cape Verde frontal zone, is mostly coupled to the southern equatorial circulation and to a much smaller extent to the Northern Atlantic gyre. Here, the net water column biological activity shows a dominantly neutral water column and little water column heterotrophy, the latter mostly confined to a region between the African coast and the Cape Verde archipelago. The intense near-surface production, the reduced gradient in productivity moving offshore (NASA-OBPG, 2010) and to some extent the transitory nature of the filaments that form on the shelf at this latitudes (Arístegui et al., 2009) result in a small impact of the organic carbon lateral fluxes. Sinking dominates the vertical export at these latitudes while mixing and vertical advection are impeded by a shallow MLD and the positive signature of the wind stress curl. In this zonal band, our model shows a weaker than observed circulation and a deeper than observed chlorophyll and NPP maximum (see section 3. Evaluation) which may lead to an underestimation of the lateral transport and therefore of the net heterotrophy of the water column. Both a shoaling of the biological production towards the surface characterized by more intense currents and an intensification of the circulation may in fact result in the strengthening of the lateral zonal and meridional organic carbon fluxes. An increase of the offshore zonal fluxes in the southern subregion could favor a more heterotrophic water column only if accompanied by an increase of the divergence of the flux, resulting in a substantial accumulation of organic carbon compared to the local production. An intensification of the southern circulation and in particular of the Mauritanian current may likely increase the influx of organic carbon from the south into the Cape Verde frontal zone, fueling even further the respiration in this already strongly heterotrophic region.

Overall, in great part of the CanUS the lateral redistribution of organic carbon from the shelf to the open waters results in a lateral shift of the deep organic carbon sinks from the regions of high organic carbon production. This is in contrast with the representation of the organic carbon pump as a pure vertical process and highlights the fundamental importance of the lateral transport of organic carbon for the maintenance of the biological activity. Despite this lateral input of organic carbon in the first 100m, our model does not show evidence for a net heterotrophic activity in the near-surface waters, therefore suggesting that the shallow open sea is everywhere a source of organic carbon for the deeper layers. Vertical integration through the mean euphotic layer depth (100m), through the punctual euphotic layer depth and through the punctual MLD (generally shallower than the euphotic layer) all agree on the net autotrophic surface ocean hypothesis (Williams et al., 2013). The spatial pattern of modeled near-surface autotrophic activity (Figure 6b from Section 4.1) seems to agree with the "Calculated global distribution of NCP" from Williams et al. (2013) Figure 1, once the net heterotrophic regions are substituted by weakly autotrophic low productive waters. The depth at which vertically integrated sinks and sources from top to bottom compensate each other in the model is almost everywhere located at more than 200m depth and can be deeper than 1000 m in regions of nearly neutral water column, confirming the importance of the respiration in deep waters (Giorgio and Duarte, 2002).

Both the mean Ekman transport and the turbulent mesoscale activity contribute to the total lateral fluxes of organic carbon connecting coastal sources to deep offshore sinks. The two concur also in determining the vertical downwelling and mixing that increase of the carbon availability at depth. The magnitude of the relative contribution of these two terms to the organic carbon fluxes and their different role in fueling the heterotrophic activity offshore must be detangled through further analysis.

Biogeosciences Discuss., doi:10.5194/bg-2016-548, 2017
Manuscript under review for journal Biogeosciences
Published: 11 January 2017

6 Conclusions

This paper provides a first comprehensive quantification of the lateral and vertical fluxes of organic carbon in the Canary Upwelling System (CanUS) up to 2000km offshore. The net community production vertically-integrated through the whole water column, i.e., $\int$NCP, reveals a net autotrophy ($\int$NCP>0) of the productive CanUS shelf and a net heterotrophy ($\int$NCP<0) of the offshore waters. However, the shallow heterotrophic layer acts everywhere as an organic carbon source, i.e., is autotrophic. The horizontal displacement of major shallow sources and major deep sinks of organic carbon must be explained by an significant lateral redistribution of the organic carbon.

Long-range lateral fluxes of organic carbon in the euphotic layer (0m-100m depth) of the CanUS are dominated by the offshore flux that extends on average as far as 1500km into the North Atlantic Gyre. Along its way, the offshore flux adds to the euphotic layer an amount of organic carbon that corresponds from 8 % to 34% of the alongshore average NCP, explaining from 62% to 80% of the excess vertical export, i.e., the export below the euphotic layer that exceeds the local production, and fueling extra heterotrophic activity at depth. In the 100m-200m layer the offshore transport of organic carbon continues to dominate the lateral fluxes, transporting always >8% of the available organic carbon and intensifies away from the coast with potential repercussions on the biological activity of the North Atlantic Gyre interior.

Strong subregional differences in the fluxes characterize the CanUS. Above the Cape Verde frontal zone, coastal production declines quickly offshore and turns into a net water column heterotrophy of the open waters. Here, the sharp peak of negative $\int$NCP is fueled by a strong offshore transport near the coast likely favored the local abundance of mesoscale filaments. Mixing and vertical downwelling play an important role in the vertical export in this subregion, potentially allowing the export of light and dissolved organic matter below the euphotic layer. Below the Cape Verde frontal zone high levels of near-surface production extend far offshore. Despite being the most productive area, the southern subregion is characterized by a modest impact of the offshore flux on the local carbon availability that results in an almost neutral water column ($\int$NCP$\sim$0). Vertical export at depth in this subregion is carried on mostly by sinking fluxes due to the shallow MLD and the positive wind stress curl signature.

The central zonal band of the CanUS located above the Cape Verde frontal zone and bridging the northern and southern subregions is characterized by an alongshore convergence of organic carbon on the shelf. The accumulated organic carbon is laterally exported from the shelf by an intense offshore flux that along the way releases on average as much organic carbon as 57% of the local NCP, fueling the most intense peak of water column heterotrophy of the CanUS. The offshore transport is pronounced also at depth especially in the first 500km from the coast, while advective and mixing fluxes have an important role in the vertical export in this subregion. Both the intense offshore transport and downwelling of organic carbon may be enhanced by the giant Cape Blanc filament.

Our study highlights the strength of the coupling between the productive CanUS region and the adjacent oligotrophic open North Atlantic. Lateral fluxes, especially the offshore transport, are influenced by mean circulation, mesoscale activity and physical forcings and have an essential role in the fueling of the open sea heterotrophic activity. Their impact on the local carbon availability fully explains the complex pattern of net sources and sinks of organic carbon of the CanUS region.

Biogeosciences Discuss., doi:10.5194/bg-2016-548, 2017
Manuscript under review for journal Biogeosciences
Published: 11 January 2017

Appendix A: Datasets

a) Forcing datasets

Data source	Ref. time	Resolution	Variables	Reference
Era-Interim	1979-2010	N128 reduced Gaussian grid	freshwater flux, wind stress, net heat flux, net shortwave radiation	Dee et al. (2011)
GLOBALVIEW 2011	1998-2011	1°x 1°grid	atmospheric pCO_2	GLOBALVIEW-CO_2 (2011)

b) Datasets used for corrections to the forcing datasets

Data source	Ref. time	Resolution	Variables	Reference
DFS 5.2	1979-2011	0.7°x 0.7°grid	downward longwave radiation, downward shortwave radiation	Brodeau et al. (2010)
Era-Interim	1979-2011	0.75°x 0.75°grid	downward longwave radiation, downward shortwave radiation	Dee et al. (2011)
Era-Interim	1989-2009	1.5°x 1.5°grid	sea-ice fraction	Dee et al. (2011)
NSIDC Sea Ice Motion Vectors	1979-2006	25 km EASE-Grid	sea-ice drift	Fowler (2003)

Table A1. Description of the datasets used for (a) the model run main forcing, (b) datasets used for calculating stratus cloud an sea ice corrections to the main forcing. DFS: Drakkar Frocing Set; NSIDC: National Snow and Ice Data Center.

Boundary conditions

Data source	Ref. time	Resolution	Variables	Reference
WOA 2013	1955-2012	0.25°x 0.25°grid	temperature, salinity, nitrate	Locarnini et al. (2013), Zweng et al. (2013)
SODA v1.4.2	1958-2001	0.5°x 0.5°grid	momentum components, sea surface height	Carton and Giese (2008)
SeaWiFS	1997-2010	9km grid	sea surface chlorophyll	NASA-OBPG (2010)
GLODAP	-	1°x 1°grid	sea surface alkalinity, sea surface dissolved inorganic carbon	Key et al. (2004)

Table A2. Description of the datasets used for the model run lateral boundary conditions. WOA: World Ocean Atlas; SODA: Simple Ocean Data Assimilation; SeaWiFS: Sea-viewing Wide Field-of-view Sensor; GLODAP: GLobal Ocean Data Analysis Project.

Biogeosciences Discuss., doi:10.5194/bg-2016-548, 2017
Manuscript under review for journal Biogeosciences
Published: 11 January 2017

Model evaluation

Data source	Ref. time	Resolution	Variables	Reference
Aviso CMDT Rio05	1993-1999	0.5°x 0.5°grid	sea surface height	Rio and Hernandez (2004)
AVHRR	1981-2014	0.25°x 0.25°grid	sea surface temperature	Reynolds et al. (2007)
CARS	1955-2003	0.5°x 0.5°grid	sea surface salinity	Ridgway et al. (2002)
Argo DT-0.2	1941-2008	2°x 2°grid	mixed layer depth	Montégut et al. (2004)
Drifters	1979-2012	0.5°x 0.5°grid	sea surface height	Lumpkin and Johnson (2013)
SeaWiFS VGPM	1997-2010	9km grid	extrapolated net primary production	Behrenfeld and Falkowski (1997)
SeaWiFS CbPM	1997-2010	9km grid	extrapolated net primary production	Westberry et al. (2008)
Modis-Aqua VGPM	2002-2016	9km grid	extrapolated net primary production	Behrenfeld and Falkowski (1997)
SeaWiFS	1997-2010	9km grid	sea surface chlorophyll	NASA-OBPG (2010)
WOD09	-	rebinned to 0.5°x 0.5°grid	chlorophyll	Johnson et al. (2009)

Table A3. Description of the datasets used for the model evaluation. CMDT: Combined Mean Dynamic Topography; AVHRR: Advanced Very High Resolution Radiometer; CARS: CSIRO Atlas of Regional Seas; SeaWiFS: Sea-viewing Wide Field-of-view Sensor; WOD09: World Ocean Database 2009.

Biogeosciences Discuss., doi:10.5194/bg-2016-548, 2017
Manuscript under review for journal Biogeosciences
Published: 11 January 2017

Appendix B: Supplementary figures

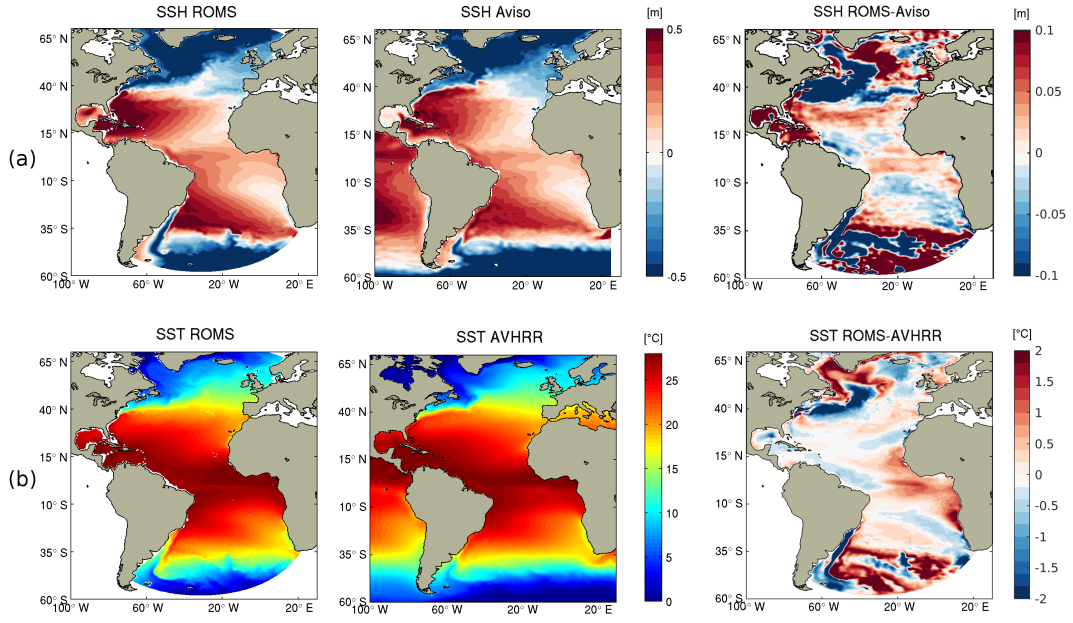

Figure B1. Mean Sea Surface Height SSH (a) and Sea Surface Temperature SST (b) from model and observational data, accompanied by a model-data difference plot in the full Atlantic Telescopic Grid domain. A detailed description of the data used for the evaluation is provided in Appendix A: Datasets, Table A3.

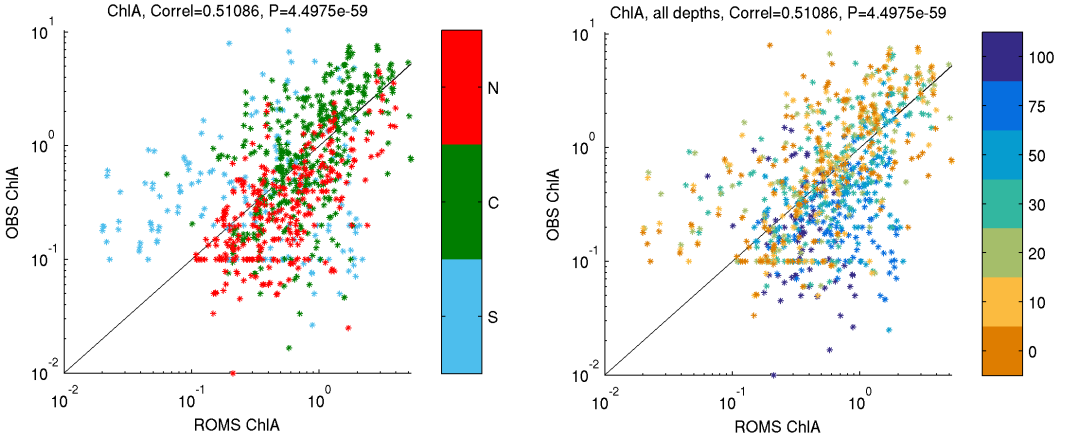

Figure B2. Evaluation of the modeled annual mean Chlorophyll by subregion and depth for the first 500km offshore as defined by the first two budget analysis boxes, see *Figure 4*. Observational dataset used for comparison: WOD09, annual mean Chlorophyll. A detailed dscription of the data used for the evaluation is provided in Appendix A: Datasets, Table A3.

Biogeosciences Discuss., doi:10.5194/bg-2016-548, 2017
Manuscript under review for journal Biogeosciences
Published: 11 January 2017

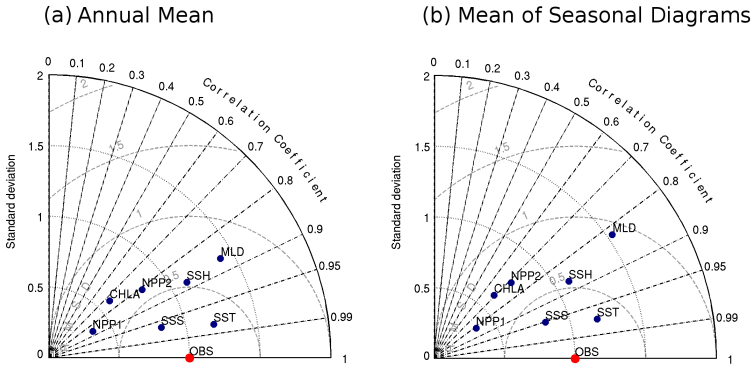

Figure B3. Taylor diagrams for the Canary EBUS region of analysis ([9.5N,32.5N]x[5W,35W]). Subplot (a) Taylor diagram of the climatological annual mean fields; Subplot (b) Mean of the four Taylor diagrams obtained for each season from climatological seasonal mean fields. Used datasets - Sea Surface Temperature (SST): AVHRR, Sea Surface Salinity (SSS): CARS, Sea Surface Height (SSH): Aviso CMDT Rio05, Mixed Layer Depth (MLD): Argo DT-0.2, Chlorophyll (CHLA): SeaWiFS, Net Primary Production dataset 1 (NPP1): SeaWiFS VGPM, Net Primary Production dataset 2 (NPP2): SeaWiFS CbPM. A detailed description of the data used for the evaluation is provided in Appendix A: Datasets, Table A3.

Author contributions. N.G., Z.L. and E.L. conceived the study. E.L. and M.M. set up the experiment and improved the model. E.L. performed the analysis. E.L. and N.G. wrote the manuscript. All authors contributed to the interpretation of the results and to the manuscript. N.G. and M.M. supervised this study.

"The authors declare that they have no conflict of interest."

Acknowledgements. We would like to thank Martin Frischknecht for his valuable comments on the work and during the preparation of the manuscript, and Damian Loher for the technical support. We also thank the group of the Faculty of Marine Sciences at the University of Las Palmas de Gran Canaria in particular Javier Arístegui for allowing a fruitful exchange of ideas and information and Bàrbara Barceló for her kind support. A special thought goes to the late professor Pablo Sangrà whose generosity and dedication to science will always be a source of inspiration. This research was financially supported by the Swiss Federal Institute of Technology Zürich (ETH Zürich) and the Swiss National Science Foundation (Project CALNEX, grant No.149384). The simulations were performed at the HPC cluster of ETH Zürich, Euler, which is located in the Swiss Supercomputing Center (CSCS) in Lugano and operated by ETH ITS Scientific IT Services in Zurich. Model output is available upon request. Please contact the corresponding author, Elisa Lovecchio (elisa.lovecchio@usys.ethz.ch), in that matter.

Biogeosciences Discuss., doi:10.5194/bg-2016-548, 2017
Manuscript under review for journal Biogeosciences
Published: 11 January 2017

References

Alonso-González, I. J., Arístegui, J., Vilas, J. C., and Hernández-Guerra, A.: Latral POC transport and consumption in surface and deep waters of the Canary Current region: a box model, Global Biogeohemical Cycles, 23, GB2007, doi:10.1029/2008GB0, 2009.

Alonso-González, I. J., Arístegui, J., Lee, C., Sanchez-Vidal, A., Calafat, A., Fabrés, J., Sangrá, P., Masquá, P., and Hernández-Guerra, A.: Role of slowly settling particles in the ocean carbon cycle, Geophysical Research Letters, 37, doi:10.1029/2010GL043827, 2010.

Álvarez Salgado, X. A., Arístegui, J., Barton, E. D., and Hansell, D. A.: Contribution of upwelling filaments to offshore carbon export in the subtropical Northeast Atlantic Ocean, Limnology and Oceanography, 52, 1287–1292, doi:10.4319/lo.2007.52.3.1287, 2007.

Arístegui, J., Barton, E. D., Montero, M. F., nos, M. G.-M., and Escánez, J.: Organic carbon distribution and water column respiration in the NW African-Canaries Coastal Transition Zone, Aquatic Microbial Ecology, 33, 289–301, doi:10.3354/ame033289, 2003.

Arístegui, J., Barton, E. D., Álvarez Salgado, X. A., Santos, M. P., Figueiras, F. G., Kifani, S., Hernández-León, S., Mason, E., Machú, E., and Demarq, H.: Sub-regional ecosystem variability in the Canary Current upwelling, Progress in Oceanography, 83, 33–48, doi:http://dx.doi.org/10.1016/j.pocean.2009.07.031, 2009.

Arítegui, J., Duarte, C. M., Agustí, S., Doval, M., Álvarez Salgado, X., and Hansell, D.: Dissolved Organic Carbon Support of Respiration in the Dark Ocean, Science,, 298, 1967, doi:10.1126/science.1076746, 2002.

Auger, P. A., Gorgues, T., Machu, E., Aumont, O., and Brehmer, P.: What drives the spatial variability of primary productivity and matter fluxes in the North-West African upwelling system? A modelling approach and box analysis, Biogeociences Discussion, 13, 6419–6440, doi:10.5194/bg-13-6419-2016, http://www.biogeosciences.net/13/6419/2016/, 2016.

Aumont, O., Maier-Reimer, E., Blain, S., and Monfray, P.: An ecosystem model of the global ocean including Fe, Si, P colimitations, Global Biogeochemical Cycles, 17, n/a–n/a, doi:10.1029/2001GB001745, http://dx.doi.org/10.1029/2001GB001745, 1060, 2003.

Barton, E. D., Arístegui, J., Tett, P., and Navarro-Pérez, E.: Variability in the Canary Islands area of filament-eddy exchanges, Progress in Oceanography, 62, 71–94, 2004.

Behrenfeld, M. J. and Falkowski, P. G.: Photosynthetic rates derived from satellite-based chlorophyll concentration, Limnology and Oceanography, 42, 1–20, doi:10.4319/lo.1997.42.1.0001, seaWiFS VGPM available at: http://orca.science.oregonstate.edu/1080.by.2160.monthly.hdf.vgpm.s.chl.a.sst.php, Modis-Aqua VGPM available at: http://orca.science.oregonstate.edu/1080.by.2160.monthly.hdf.vgpm.m.chl.m.sst.php, 1997.

Berelson, W. M.: Particle settling rates increase with depth in the ocean, Deep-Sea Research II: Topical Studies in Oceanography, 49, 237–251, doi:http://dx.doi.org/10.1016/S0967-0645(01)00102-3, 2002.

Brochier, T., Mason, E., Moyano, M., Berraho, A., Colas, F., Sangrá, P., Hernández-León, S., Ettahiri, O., and Lett, C.: Ichtyoplankton transport from the African coast to the Canary Islands, Journal of Marine Systems, 87, 109–122, 2014.

Brodeau, L., Barnier, B., Treguier, A.-M., Penduff, T., and Gulev, S.: An ERA40-based atmospheric forcing for global ocean circulation models, Ocean Modelling, 31, 88–104, doi:http://dx.doi.org/10.1016/j.ocemod.2009.10.005, 2010.

Carr, M.-E.: Estimation of potential productivity in the Eastern Boundary Currents using remote sensing, Deep-Sea Research II: Topical Studies in Oceanography, 49, 59–80, doi:http://dx.doi.org/10.1016/S0967-0645(01)00094-7, 2002.

Carr, M.-E. and Kearns, E. J.: Production regimes in four Eastern Boundary Current Systems, Deep-Sea Research II, 50, 3199–3221, doi:http://dx.doi.org/10.1016/j.dsr2.2003.07.015, 2003.

Carton, J. A. and Giese, B. S.: A Reanalysis of Ocean Climate Using Simple Ocean Data Assimilation (SODA), American Meteorological Society, Monthly Weather Review, 136, 2999–3017, doi:http://dx.doi.org/10.1175/2007MWR1978.1, 2008.

Chavez, F. P. and Messié, M.: A comparison of Eastern Boundary Upwelling Ecosystems, Progress in Oceanography, 83, 80–96, doi:http://dx.doi.org/10.1016/j.pocean.2009.07.032, 2009.

Dai, A., Qian, T., Trenberth, K. E., and Milliman, J. D.: Changes in continental freshwater discharge from 1948-2004, Journal of Climate, American Meteorological Society, 22, 2773–2791, doi:http://dx.doi.org/10.1175/2008JCLI2592.1, dataset: http://www.cgd.ucar.edu/cas/catalog/surface/dai-runoff/, 2009.

Dee, D. P., Uppala, S. M., Simmons, A. J., P. Berrisford, P. P., Kobayashi, S., Andrae, U., Balmaseda, M. A., G. Balsamo, P. B., P. Bechtold, A. C. M. B., van de Berg, L., Bidlot, J., Bormann, N., Delsol, C., Dragani, R., Fuentes, M., Geer, A. J., Haimberger, L., Healy, S. B., Hersbach, H., Hólm, E. V., Isaksen, L., P. Kallberg, M. K., Matricardi, M., McNally, A. P., B. M. Monge-Sanz, J.-J. M., B.-K. Park, C. P., de Rosnay, P., Tavolato, C., n. Thépaut, J., and Vitart, F.: The ERA-Interim reanalysis: configuration and performance of the data assimilation system, Quarterly Journal of the Royal Meteorolgical Society, 137, 553–597, doi:http://onlinelibrary.wiley.com/doi/10.1002/qj.828/abstract, 2011.

Del Giorgio, P. A. and Duarte, C. M.: Respiration in the open ocean, Nature, 420, 379–384, doi:doi:10.1038/nature01165, http://www.nature.com/nature/journal/v420/n6914/full/nature01165.html, 2002.

Duarte, C. M. and Agustí, S.: The CO_2 Balance of Unproductive Aquatic Ecosystems, Science, 281, 234–236, doi:10.1126/science.281.5374.234, http://science.sciencemag.org/content/281/5374/234, 1998.

Duarte, C. M. and Cebrián, J.: The fate of marine autotrophic production, Limnology and Oceanography, 41, 1758–1766, doi:10.4319/lo.1996.41.8.1758, 1996.

Duarte, C. M., de Gioux, A. R., Arrieta, J. M., Delgado-Huertas, A., and Augustí, S.: The Oligotrophic Ocean is Heterotrophic, Annual Review of Marine Science, 5, 551–569, 2013.

Ducklow, H. W. and Doney, S. C.: What is the metabolic state of the oligotrophic ocean? A Debate, Annual Review of Marine Science, 5, 525–533, doi:10.1146/annurev-marine-121211-172331, 2013.

Ducklow, H. W., Steinberg, D. K., and Buesseler, K.: Upper ocean Carbon Export and the Biological Pump, Oceanography, 14, 50–58, doi:http://dx.doi.org/10.5670/oceanog.2001.06, 2001.

Dussin, R., Barnier, B., Brodeau, L., and Molines, J. M.: The Making Of the Drakkar Forcing Set DFS5, Tech. rep., LGGE, Grenoble, France, https://www.drakkar-ocean.eu/publications/reports/report_DFS5v3_April2016.pdf, 2016.

Falkowski, P. G., Biscaye, P. E., and Sancetta, C.: The lateral flux of biogenic particles from the eastern North American continental margin to the North Atlantic Ocean, Deep-Sea Research II: Topical Studies in Oceanography, 41, 583–601, doi:http://dx.doi.org/10.1016/0967-0645(94)90036-, http://www.sciencedirect.com/science/article/pii/0967064594900361, 1994.

Fischer, G., Reuter, C., Karakas, G., Nowald, N., and Wefer, G.: Offshore advection of particles within the Cape Blanc filament, Mauritania: Results from observational and modelling studies, Progress in Oceanography, 83, 322–330, doi:http://dx.doi.org/10.1016/j.pocean.2009.07.023, 2009.

Fischer, J. and Karakaş, G.: Sinking rates and ballast composition of particles in the Atlantic Ocean: implications for the organic carbon fluxes to the deep ocean, Biogeosciences, 6, 85–102, doi:10.5194/bg-6-85-2009, 2009.

Fowler, C.: Polar Pathfinder Daily 25 km EASE-Grid Sea Ice Motion Vectors (1979-2006), Tech. rep., Boulder, Colorado USA: National Snow and Ice Data Center, http://nsidc.org/data/docs/daac/nsidc0116_icemotion.gd.html(accessedMar2012), updated 2008, 2003.

Gabric, A. J., Garcia, L., Camp, L. V., Nykjaer, L., Eifler, W., and Schrimpf, W.: Offshore export of shelf production in the Cape Blanc (Mauritania) giant filament as derived from coastal zone color scanner imagery, Journal of Geophysical Research, 98, 4697–4712, doi:10.1029/92JC01714, 1993.

Galbraith, E. D., Gnanadesikan, A., Dunne, J. P., and Hiscock, M. R.: Regional impacts of iron-light colimitation in a global biogeochemical model, Biogeosciences, 7, 1043–1064, doi:10.5194/bg-7-1043-2010, http://www.biogeosciences.net/7/1043/2010/, 2010.

García-Muñoz, M., Arístegui, J., Pelegrí, J. L., Antoranz, A., Ojeda, A., and Torres, M.: Exchange of carbon by an upwelling filament off Cape Ghir (NW Africa), Journal of Marine System, 54, 83–95, doi:http://dx.doi.org/10.1016/j.jmarsys.2004.07.005, 2005.

Giorgio, P. A. D. and Duarte, C. M.: Respiration in the open ocean, Nature, 420, 379–384, doi:10.1038/nature01165, 2002.

GLOBALVIEW-CO_2: Cooperative Atmospheric Data Integration Project – Carbon Dioxide, Tech. rep., NOAA ESRL, Boulder Colorado, https://www.esrl.noaa.gov/gmd/ccgg/globalview/co2/co2_download.html, 2011.

Gruber, N., Frenzel, H., Doney, S. C., Marchesiello, P., McWilliams, J. C., Oram, J. R., Plattner, G. K., and Stolzenbach, K. D.: Eddy-resolving simulation of plankton ecosystem dynamics in the California Current System, Deep Sea Research I: Oceanographic Research Papers, 53, 1483–1516, doi:http://dx.doi.org/10.1016/j.dsr.2006.06.005, 2006.

Gruber, N., Lachkar, Z., Frenzel, H., Marchesiello, P., Münnich, M., McWilliams, J. C., Nagai, T., and Plattner, G.-K.: Eddy-induced reduction of biological production in eastern boundary upwelling systems, Nature Geoscience, 4, 787–792, doi:10.1038/ngeo1273, 2011.

Hansell, D. A.: DOC in the Global Ocean Carbon Cycle, vol. Chap.15, Academic Press - Elsevier, biogeochemistry of marine dissolved organic matter edn., pp.685-714, cp1-cp4, 2002.

Haumann, F. A., Gruber, N., Münnich, M., Frenger, I., and Kern, S.: Sea-ice transport driving Southern Ocean salinity and its recent trends, Nature, 537, 89–92, doi:10.1038/nature19101, 2016.

Hauri, C., Gruber, N., Vogt, M., Doney, S. C., Feely, R. A., Lachkar, Z., Leinweber, A., McDonnell, A. M. P., Munnich, M., and Plattner, G.-K.: Spatiotemporal variability and long-term trends of ocean acidification in the California Current System, Biogeosciences, 10, 193–216, doi:10.5194/bg-10-193-2013, http://www.biogeosciences.net/10/193/2013/, 2013.

Helmke, P., Romero, O., and Fischer, G.: Northwest African upwelling and its effect on offshore organic carbon export to the deep sea, Global Biogeochemical Cycles, 19, GB4015, doi:10.1029/2004GB002265, 2005.

Hopkinson, S. and Vallino, J. J.: Efficient export of carbon to the deep ocean through dissolved organic matter, Nature, 433, 142–145, doi:10.1038/nature03191, 2005.

Hwang, J., Druffel, E. R. M., and Komada, T.: Transport of organic carbon from the California coast to the slope region: A study of Δ^{14}C and Δ^{13} C signatures of organic compound classes, Global Biogeochem. Cycles, 19, doi:10.1029/2004GB002347, 2008.

Inthorn, M., Mohrholz, V., and Zabel, M.: Nepheloid layer distribution in the Benguela upwelling area offshore Namibia, Deep Sea Research I: Oceanographic Research Papers, 53, 1423–1438, doi:http://dx.doi.org/10.1016/j.dsr.2006.06.004, 2006a.

Inthorn, M., Wagner, T., Scheeder, G., and Zabel, M.: Lateral transport controls distribution, quality and burial of organic matter along ocontinental slopes in high-productivity areas, Geology, 34, 205–208, doi:10.1130/G22153.1, 2006b.

Johnson, D. R., Boyer, T. P., Garcia, H. E., Locarnini, R. A., Baranova, O. K., and Zweng, M. M.: World Ocean Database 2009 Documentation, Tech. rep., Edited by Sydney Levitus, NODC Internal Report 20, NOAA Printing Office, Silver Spring, MD, 175 pp., http://www.nodc.noaa.gov/OC5/WOD09/pr_wod09.html, 2009.

Key, R. M., Kozyr, A., Sabine, C. L., Lee, K., Wanninkhof, R., Bullister, J., Feely, R. A., Millero, F., Mordy, C., and Peng, T.-H.: A global ocean carbon climatology: Results from GLODAP, Global Biogeochemical Cycles, 18, GB4031, doi:10.1029/2004GB002247, 2004.

Lachkar, Z. and Gruber, N.: What controls biological production in coastal upwelling systems? Insights from a comparative modeling study, Biogeosciences, 8, 2961–2976, doi:10.5194/bg-8-2961-2011, 2011.

Lachkar, Z. and Gruber, N.: Response of biological production and air–sea CO_2 fluxes to upwelling intensification in the California and Canary Current Systems, Journal of Marine Systems, 109–110, 149 – 160, doi:http://dx.doi.org/10.1016/j.jmarsys.2012.04.003,

http://www.sciencedirect.com/science/article/pii/S092479631200108X, large-scale regional comparisons of marine biogeochemistry and ecosystem processes - research approaches and results, 2013.

Landschützer, P., Gruber, N., Bakker, D. C. E., and Schuster, U.: An observation-based global monthly gridded sea surface pCO2 product from 1998 through 2011 and its monthly climatology, Tech. rep., Carbon Dioxide Information Analysis Center, Oak Ridge National Laboratory, US Department of Energy, Oak Ridge, Tennessee, doi:10.3334/CDIAC/OTG.SPCO2_1998_2011_ETH_SOM-FFN, http://cdiac.ornl.gov/ftp/oceans/spco2_1998_2011_ETH_SOM-FFN, 2014.

Large, W. G., McWilliams, J. C., and Doney, S. C.: Oceanic vertical mixing: A review and a model with a nonlocal boundary layer parameterization, Rev. Geophys., 32, 363–403, doi:10.1029/94RG01872, 1994.

Liu, K. K., Atkinson, L., nones, R. A. Q., and Talaue-McManus, L.: Carbon and Nutrient Fluxes in Continental Margins. A Global Synthesis, Global Change - The IGBP Series, Springer-Verlag Berlin Heidelberg, 2010.

Locarnini, R. A., Mishonov, A. V., Antonov, J. I., Boyer, T. P., Garcia, H. E., Baranova, O. K., Zweng, M. M., Paver, C. R., Reagan, J. R., Johnson, D. R., Hamilton, M., and Seidov, D.: World Ocean Atlas 2013, Volume 1: Temperature, Tech. rep., S. Levitus, Ed., A. Mishonov Technical Ed.; NOAA Atlas NESDIS 73, 40 pp, http://data.nodc.noaa.gov/woa/WOA13/DOC/woa13_vol1.pdf, 2013.

Lumpkin, R. and Johnson, G. C.: Global Ocean Surface Velocities from Drifters: Mean, Variance, ENSO Response, and Seasonal Cycle, Journal of Geophysical Research: Oceans, 118, 2992–3006, doi:10.1002/jgrc.20210, 2013.

Mackas, D. L., Strub, P. T., Thomas, A., and Montecino, V.: Eastern Ocean Boundaries: Pan-Regional Overview, book: "The Sea, The Global Coastal Ocean", 14, 2006.

Montégut, C. D. B., Madec, G., Fischer, A. S., Lazar, A., and Iudicone, D.: Mixed layer depth over the global ocean: An examination of profile data and a profile-based climatology, J. Geophys. Res, 109, C12 003, doi:10.1029/2004JC002378, 2004.

Moore, J. K., Doney, S. C., and Lindsay, K.: Upper ocean ecosystem dynamics and iron cycling in a global three-dimensional model, Global Biogeochemical Cycles, 18, doi:10.1029/2004GB002220, http://dx.doi.org/10.1029/2004GB002220, gB4028, 2004.

Nagai, T., Gruber, N., Frenzel, H., Lachkar, Z., McWilliams, J. C., and Plattner, G.-K.: Dominant role of eddies and filaments in the offshore transport of carbon and nutrients in the California Current System, Journal of Geophysical Research, 120, doi:10.1002/2015JC010889, 2015.

NASA-OBPG: SeaWiFS Data Level-3 Standard Mapped Image, S19972442010273.3m_mc_chl_chlor_a_9km.nc, NASA Goddard Space Flight Center, Ocean Ecology Laboratory, Ocean Biology Processing Group, http://oceandata.sci.gsfc.nasa.gov, (1997-2010), 2010.

Ohde, T., Fiedler, B., and Körtzinger, A.: Spatio-temporal distribution and transport of particulate matter in the eastern tropical North Atlantic observed by Argo floats, Deep-Sea Research I, 102, 26–42, doi:http://dx.doi.org/10.1016/j.dsr.2015.04.007, 2015.

Pelegrí, J. L., Arístegui, J., Cana, L., González-Dávila, M., Hernández-Guerra, A., Hernández-León, S., Montero, M. F., Sangrá, P., and Santana-Casiano, M.: Coupling between the open ocean and the coastal upwelling region off northwest Africa: water recirculation and offshore pumping of organic matter, Journal of Marine Systems, 54, 3–37, doi:http://dx.doi.org/10.1016/j.jmarsys.2004.07.003, 2005.

Peliz, A., Santos, A. M. P., Oliveira, P. B., and Dubert, J.: Extreme cross-shelf transport induced by eddy interactions southwest of Iberia in winter 2001, Geophysical Research Letters, 31, L08 301, doi:10.1029/2004GL019618, 2004.

Plattner, G.-K., Gruber, N., Frenzel, H., and McWilliams, J. C.: Decoupling marine export production from new production, Geophysical Research Letters, 32, doi:10.1029/2005GL022660, http://dx.doi.org/10.1029/2005GL022660, l11612, 2005.

Reynolds, R. W., Smith, T. M., Liu, C., Chelton, D. B., Casey, K. S., and Schlax, M. G.: Daily High-Resolution-Blended analyses for sea surface temperature, J. Climate, 20, 5473–5496, doi:http://dx.doi.org/10.1175/2007JCLI1824.1, 2007.

Ridgway, K. R., Dunn, J. R., and Wilkin, J. L.: Ocean interpolation by four-dimensional least squares: Application to the waters around Australia, J. Atmos. Ocean, 19, 1357–1375, doi:http://dx.doi.org/10.1175/1520-0426(2002)019<1357:OIBFDW>2.0.CO;2, 2002.

Rio, M.-H. and Hernandez, F.: A mean dynamic topography computed over the world ocean from altimetry, in situ measurements, and a geoid model, J. Geophys. Res, 109, C12 032, doi:10.1029/2003JC002226, 2004.

Sangrà, P., Pascual, A., Rodríguez-Santana, A., F.Machín, Mason, E., McWilliams, J., Pelegrí, J., Dong, C., Rubio, A., Arístegui, J., Marrero-Díaz, A., Hernández-Guerra, A., Martínez-Marrero, A., and Auladell, M.: The Canary Eddy Corridor: A major pathway for long-lived eddies in the subtropical North Atlantic, Deep Sea Research I: Oceanographic Research Papers, 56, 2100–2114, doi:http://dx.doi.org/10.1016/j.dsr.2009.08.008, 2009.

Santana-Falcón, Y., Benavides, M., Sangrà, P., Mason, E., Barton, E. D., Orbi, A., and Arístegui, J.: Coastal-offshore exchange of organic matter across the Cape Ghir filament (NW Africa) during moderate upwelling, Journal of Marine Systems, 154, 233–242, doi:http://dx.doi.org/10.1016/j.jmarsys.2015.10.008, 2016.

Sarmiento, J. L. and Gruber, N.: Ocean Biogeochemical Dynamics, Princeton University Press, iSBN: 9781400849079, 2006.

Shchepetkin, A. F. and McWilliams, J. C.: The regional oceanic modeling system (ROMS): a split-explicit, topographic-following-coordinate oceanic model, Ocean Modeling, 9, 347–404, doi:http://dx.doi.org/10.1016/j.ocemod.2004.08.002, 2005.

Shigemitsu, M., Okunishi, T., Nishioka, J., Sumata, H., Hashioka, T., Aita, M. N., Smith, S. L., Yoshie, N., Okada, N., and Yamanaka, Y.: Development of a one-dimensional ecosystem model including the iron cycle applied to the Oyashio region, western subarctic Pacific, Journal of Geophysical Research: Oceans, 117, doi:10.1029/2011JC007689, http://dx.doi.org/10.1029/2011JC007689, c06021, 2012.

Steele, M., Mellor, G. L., and Mcphee, M. G.: Role of the Molecular Sublayer in the Melting or Freezing of Sea Ice, Journal of Physical Oceanography, 19, 139–147, doi:10.1175/1520-0485(1989)019<0139:ROTMSI>2.0.CO;2, http://dx.doi.org/10.1175/1520-0485(1989)019<0139:ROTMSI>2.0.CO;2, 1989.

Turi, G., Lachkar, Z., and Gruber, N.: Spatiotemporal variability and drivers of pCO_2 and air–sea CO_2 fluxes in the California Current System: an eddy-resolving modeling study, Biogeosciences, 11, 671–690, doi:10.5194/bg-11-671-2014, http://www.biogeosciences.net/11/671/2014/, 2014.

Váldes, L. and Déniz-González, I.: Oeanographic and biological features in the Canary Current Large Marine Ecosystem, vol. pp.115-383 of *Technical Series 115*, IOC-UNESCO, Paris, 2015.

Walsh, J. J.: Importance of continental margins in the marine biogeochemical cycling of carbon and nitrogen, Nature, 350, 53–55, doi:10.1038/350053a0, 1991.

Westberry, T., Behrenfeld, M. J., Siegel, D. A., and Boss, E.: Carbon-based primary productivity modeling with vertically resolved photoacclimation, Global Biogeochemical Cycles, 22, GB2024, doi:10.1029/2007GB003078, seaWiFS VGPM available at: http://orca.science.oregonstate.edu/1080.by.2160.monthly.hdf.cbpm2.s.php, 2008.

Williams, P. J. L. B., Quay, P. D., Westberry, T. K., and Behrenfeld, M. J.: The Oligotrophic Ocean Is Autotrophic, Annual Review of Marine Science, 5, 535–549, doi:10.1146/annurev-marine-121211-172335, 2013.

Zweng, M., Reagan, J. R., Antonov, J. I., Locarnini, R. A., Mishonov, A. V., Boyer, T. P., Garcia, H. E., Baranova, O. K., Johnson, D. R., and D. Seidov, M. M. B.: World Ocean Atlas 2013, Volume 2: Salinity, Tech. rep., S. Levitus, Ed., A. Mishonov Technical Ed.; NOAA Atlas NESDIS 74, 39 pp, http://data.nodc.noaa.gov/woa/WOA13/DOC/woa13_vol2.pdf, 2013.